nature communications

Article

https://doi.org/10.1038/s41467-024-53097-5

Secretion of endoplasmic reticulum protein VAPB/ALS8 requires topological inversion

Received: 30 March 2023

Accepted: 1 October 2024

Published online: 10 October 2024

Check for updates

Kosuke Kamemura[1], Rio Kozono[1], Mizuki Tando[1], Misako Okumura[1,2], Daisuke Koga[3], Satoshi Kusumi[4], Kanako Tamai[1], Aoi Okumura[1], Sayaka Sekine[5], Daichi Kamiyama[6] & Takahiro Chihara[1,2]

VAMP-associated protein (VAP) is a type IV integral transmembrane protein at the endoplasmic reticulum (ER). Mutations in human VAPB/ALS8 are associated with amyotrophic lateral sclerosis (ALS). The N-terminal major sperm protein (MSP) domain of VAPB (*Drosophila* Vap33) is cleaved, secreted, and acts as a signaling ligand for several cell-surface receptors. Although extracellular functions of VAPB are beginning to be understood, it is unknown how the VAPB/Vap33 MSP domain facing the cytosol is secreted to the extracellular space. Here we show that Vap33 is transported to the plasma membrane, where the MSP domain is exposed extracellularly by topological inversion. The externalized MSP domain is cleaved by Matrix metalloproteinase 1/2 (Mmp1/2). Overexpression of Mmp1 restores decreased levels of extracellular MSP domain derived from ALS8-associated Vap33 mutants. We propose an unprecedented secretion mechanism for an ER-resident membrane protein, which may contribute to ALS8 pathogenesis.

VAMP-associated protein (VAP) is an endoplasmic reticulum (ER)-resident protein required for tethering ER membranes and various intracellular organelles (Golgi apparatus, mitochondria, endosomes, peroxisomes, transport vesicles, lipid droplets, and autophagosomes) at membrane contact sites (MCSs) to maintain their structure and function[1]. Humans possess two VAPs (VAPA and VAPB). Several mutations (P56S, P56H, del160S, T46I, V234I, A145V) in human *VAPB* have been reported to be associated with amyotrophic lateral sclerosis (ALS), which is a progressive neurodegenerative disease that preferentially affects motor neurons[2–7]. VAPB is composed of an N-terminal MSP (major sperm protein) domain, a coiled-coil domain, and a C-terminal transmembrane domain. The N-terminal MSP domain of VAPB has been shown to face the cytoplasm[8] and VAPB has essentially almost no luminal residues, meaning that VAPB is a type IV integral transmembrane protein, or "tail-anchored protein". The MSP domain interacts with FFAT [two phenylalanines (FF) in an acidic tract (AT)] and FFAT-like motifs of its binding partners, such as multiple lipid-transfer proteins (e.g., NIR2, CERT, FAPP2, and OSBP) at Golgi-ER contact sites, and regulates lipid composition in the Golgi[9,10]. VAPB is also shown to be required for cell-autonomous autophagic and lysosomal degradation in *Drosophila*[11].

Apart from its intracellular functions, the MSP domain of VAPB is cleaved, secreted to the extracellular space, and has extracellular signaling functions via growth cone guidance receptors including Eph, Roundabout (Robo), and Lar-like (Lar)[1,12,13]. The cleavage of VAPB has been reported in nematode, fly, mouse, rat, and human[12–15]. In *C. elegans*, the secreted MSP domain of VPR-1 (*C. elegans* VAPB ortholog) modulates mitochondrial localization and morphology in striated muscle via SAX-3 (Robo) and CLR-1 (Lar) receptors[13]. It was recently shown that the cleaved MSP domain of VPR-1 is released from the intestine and acts in distal gonads to regulate gonad development[16]. A similar, non-cell autonomous role of the secreted MSP domain at the neuromuscular junction was documented in *Drosophila* Vap33 (the *Drosophila* ortholog of VAPB)[12,13].

[1]Program of Biomedical Science, Graduate School of Integrated Sciences for Life, Hiroshima University, Higashi-Hiroshima, Hiroshima, Japan. [2]Program of Basic Biology, Graduate School of Integrated Sciences for Life, Hiroshima University, Higashi-Hiroshima, Hiroshima, Japan. [3]Department of Microscopic Anatomy and Cell Biology, Asahikawa Medical University, Asahikawa, Hokkaido, Japan. [4]Department of Morphological Sciences, Graduate School of Medical and Dental Sciences, Kagoshima University, Kagoshima, Kagoshima, Japan. [5]Graduate School of Life Sciences, Tohoku University, Sendai, Miyagi, Japan. [6]Department of Cellular Biology, University of Georgia, Athens, GA, USA. e-mail: tchihara@hiroshima-u.ac.jp

Cell-autonomous dysfunction of VAPB has been considered one of the pathomechanisms underlying ALS disease. Expression of an ALS8-associated mutant VAPB^{P56S} in HeLa cells causes VAPB aggregation in the ER, and endogenous VAP is trapped in the mutant aggregates[17]. *Drosophila* Vap33 with a P58S mutation, which corresponds to the human P56S mutation, displays similar phenomena in motor neurons[12]. Thus, it has been suggested that P56S proteins cause motor neuron degeneration by dominant-negative effects in the ALS patients. ALS is also characterized by changes in the non-cell autonomous components. In cerebrospinal fluid, the VAPB MSP domain was absent in 58.7% of sporadic ALS patients[18], suggesting abnormal VAPB processing and secretion in the brain. VAPB^{P56S} is resistant to proteolysis in primary cultures of rat hippocampal cells[15]. *Drosophila* Vap33 with a P58S mutation fails to be secreted in wing imaginal disc and S2 cells[12]. These reports suggest that impairment of VAPB extracellular functions contributes to the pathogenesis of ALS[19].

Although increasing evidence implicates the secreted MSP domain of VAPB as an important signaling ligand with physiological and pathological roles, the underlying mechanism by which the MSP domain is secreted is largely a mystery. A recent in vivo RNAi-based screen using *C. elegans* identified *ykt-6* as one of the molecules involved in secretion of the VPR-1 MSP domain[20]. Ykt6 is a SNARE protein functioning in various intracellular trafficking pathways, including transportation between ER and Golgi[21,22]. Ykt6 is also required for the exosomal secretory pathway, which is one arm of unconventional protein secretion[23,24]. Because of the promiscuous nature of Ykt6, the secretory pathway responsible for Vap33 secretion remains unknown.

The topology of a sequentially inserted transmembrane protein is defined by the location of the N- and C-termini of the membrane-spanning polypeptide chain with respect to the inner or outer side of the membrane. Adopting a proper topology is important for the physiological functions of a membrane protein. Some proteins even adopt a dual topology and exhibit functional duality[25,26]. The topology at the ER membrane is tightly related to protein secretion. Generally, a secretory protein has an N-terminal signal peptide which targets the protein into the ER lumen, and the protein is then secreted through the ER to Golgi-dependent conventional secretion pathway. However, VAPB protein does not have an N-terminal signal peptide and directs the N-terminal MSP domain into the cytosol at the ER membrane[8]. How VAPB releases the cytosolic MSP domain and where the cleavage event occurs is unknown.

In this study, we investigated the secretion mechanism of VAPB using in vitro studies of *Drosophila* Vap33. We show that ER-resident Vap33 protein is transported to the plasma membrane, where Vap33 inverts its topology to externalize the MSP domain to the extracellular space. The MSP domain is then cleaved by Matrix metalloproteinase 1/2 (Mmp1/2), which are membrane-bound or secreted proteinases that cleave extracellular proteins. The levels of secreted MSP domain of mutant Vap33$^{P58S/T48I}$ were restored by overexpression of Mmp1/2, suggesting that the precise control of Mmp1/2 activity may be a potential therapeutic strategy for ALS.

Results

Vap33 integrated into the ER membrane directs the MSP domain to the cytosol

Whether secretory proteins face the ER lumen or not has important implications for the protein secretion pathway. The domains initially facing the cytosol maintain this topology during subsequent vesicular trafficking, budding and fusion events, and these domains always face the cytoplasm even during intracellular transport. To examine the topology of *Drosophila* Vap33 on the ER membrane, we utilized a split-GFP system[27–29]. We fused GFP11 on the N-terminus of Vap33 to generate GFP11-Vap33-HA construct and co-expressed it with cytosolic GFP1-10 (GFP1-10^{cyto}) or ER-localized GFP1-10 (GFP1-10ER; SP::GFP1-10::SEHDEL) in S2 cells. We found that GFP11-Vap33-HA emitted a strong GFP signal when co-expressed with GFP1-10^{cyto}, but a significantly weaker signal when co-expressed with GFP1-10ER (Fig. 1a–c). This result indicates that most Vap33 proteins on the ER membrane direct the MSP domain to the cytosol, consistent with a type IV topology.

To further investigate the topology of Vap33 on the ER membrane, we examined *N*-glycosylation status of Vap33. *N*-glycosylation is one of the major post-translational modifications occurring within the ER lumen. To monitor the N-terminus and C-terminus of Vap33, Vap33 was fused with a FLAG-tag and an HA-tag at the N- and C-termini, respectively (FLAG-Vap33-HA). Overexpression of FLAG-Vap33-HA using *Actin-Gal4* almost completely rescued the pharate adult lethality associated with the *vap33^{43I}* mutant fly (Supplementary Table 1), indicating the FLAG-Vap33-HA fusion protein retains the molecular function of Vap33. As a positive control, we artificially fused a signal peptide to the N-terminus of FLAG-Vap33-HA (ss-Vap33) and GFP11-Vap33-HA (ss-FLAG-GFP11-Vap33). ss-FLAG-GFP11-Vap33 exhibited significant GFP fluorescent signal when co-expressed with GFP1-10ER, but not when co-expressed with GFP1-10^{cyto} (Fig. 1d–f), indicating the signal peptide is functional. The cell lysates extracted from S2 cells expressing Vap33 or ss-Vap33 were treated with *N*-glycosidase PNGaseF and analyzed by Western blotting. The PNGaseF treatment shifted the full-length band of ss-Vap33 to one of lower molecular weight, indicating that Vap33 is a potential target of *N*-glycosylation (Fig. 1g). On the other hand, the molecular weight of wild-type Vap33 was not altered upon PNGaseF treatment (Fig. 1g). These results again demonstrate that the MSP domain of Vap33 is in the cytosol, but not in the ER lumen.

Vap33 inverts its topology and directs the MSP domain extracellularly on the plasma membrane

Tsuda et al.[12] demonstrated that the MSP domain of the Vap33 protein exists in the extracellular space in the wing-imaginal disc cells of *Drosophila*[12]. As reported previously[12], we found that extracellular staining (without detergents) of the wing disc expressing FLAG-Vap33-HA with anti-FLAG and anti-HA antibody showed strong FLAG signals but faint HA signals (Fig. 2a), indicating that the MSP domain of most of the surface-localized Vap33 was extracellularly localized. To assess the proportion of cells expressing the inverted Vap33 on the cell surface, we transfected S2 cells with EGFP-T2A-FLAG-Vap33-HA plasmid and performed extracellular staining with mouse anti-FLAG mouse antibody and anti-mouse IgG Alexa 555 antibody (Fig. 2b). We counted cells with EGFP or FLAG signal and quantified the percentage of EGFP+ cells emitting extracellular FLAG signal. The results showed that 19.2% of transfected cells exposed the MSP domain extracellularly (Fig. 2b and Supplementary Table 2).

If the Vap33 MSP domain that faces the cytosol on the ER membrane is transported to the plasma membrane via the vesicular network, the Vap33 MSP domain on the plasma membrane would be expected to direct to the cytosol. However, as shown in Fig. 2a, b, the existence of the MSP domain in the extracellular space suggests the hypothesis that Vap33 protein inverts its membrane topology to direct the MSP domain extracellularly. This hypothesis is against the central dogma of membrane biology, which assumes that the initial topology of a protein at the ER membrane accurately reflects the topology of the protein elsewhere in the cell, and that the topology is conserved during vesicular trafficking[30]. However, co-translational, post-translational, and even post-insertional inversions of topologies are previously reported[31–33].

To biochemically confirm whether Vap33 inverts its topology at the plasma membrane, we carried out cell-surface biotinylation assays. The S2 cells expressing FLAG-Vap33-HA, cytosolic GFP, or FLAG-Histone H3 were reacted with membrane-impermeable biotinylation reagents. After cells were lysed, the biotinylated proteins were collected by streptavidin beads, and eluted samples were analyzed by

https://doi.org/10.1038/s41467-024-53097-5

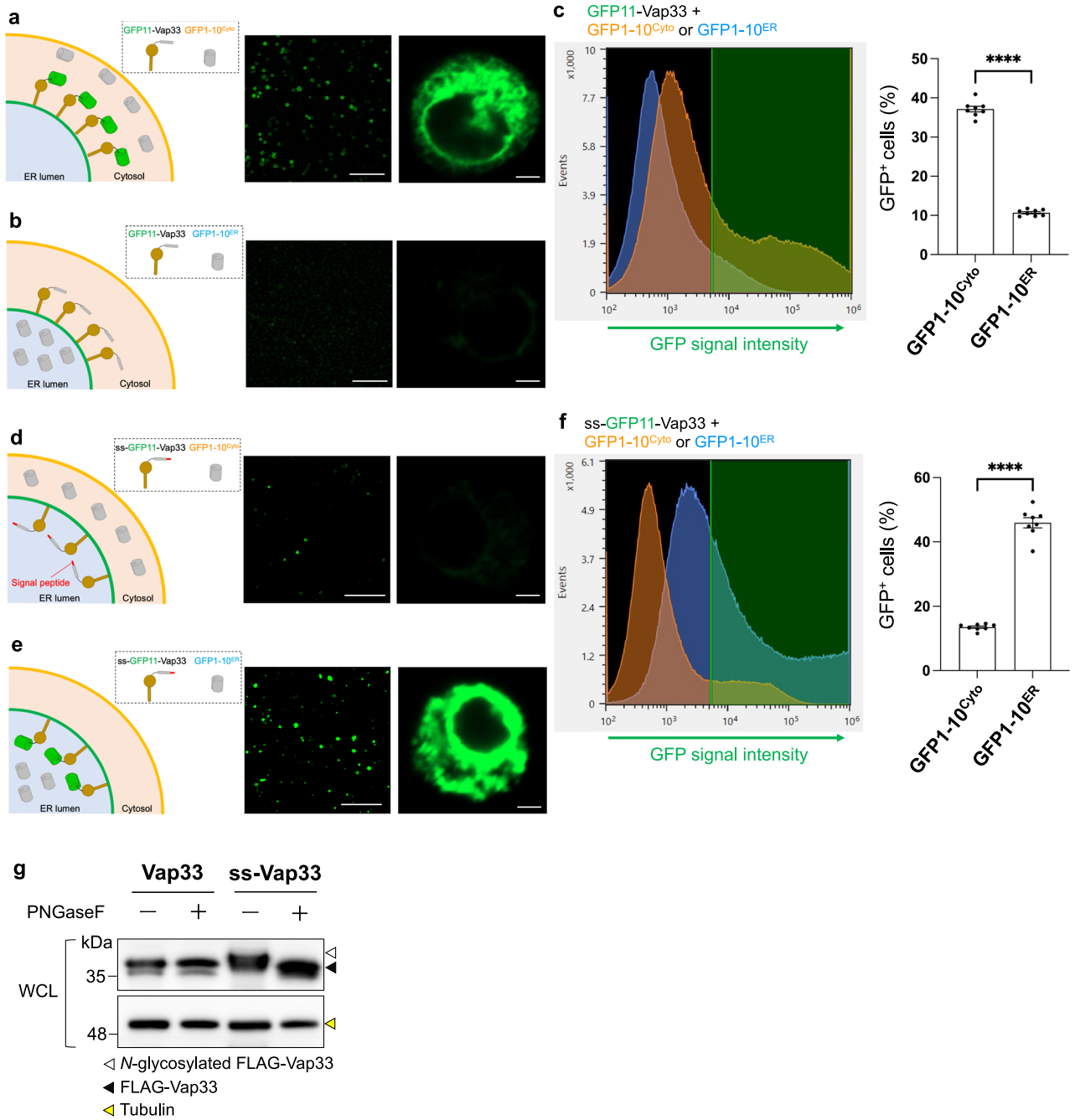

Fig. 1 | Vap33 on the ER membrane directs its MSP domain into cytosol. GFP11-Vap33-HA (**a**–**c**) and ss-FLAG-GFP11-Vap33-HA (**d**–**f**) were co-expressed with GFP1-10^{Cyto} (**a**, **d**) or GFP1-10ER (**b**, **e**) in S2 cells, and the GFP fluorescence was analyzed by laser-scanning confocal microscope (**a**, **b**, **d**, **e**) and flow cytometry (**c**, **f**). The results were reproduced in three biologically independent experiments. Scale bars of low and high magnification are 100 μm and 2 μm, respectively. **c**, **f** Orange and blue histogram show the cells co-expressing GFP1-10^{Cyto} or GFP1-10ER, respectively. The percentage of the cells in the green area was used to compare the GFP$^+$ cells. Statistical analysis was performed with the unpaired t-test (****$P < 0.0001$, two-sided). Error bars represent the standard error of the mean (SEM) of 8 biologically independent experiments ($n = 8$). **g**, *N*-glycosidase (PNGase F) sensitivity of Vap33 and ss-Vap33 expressed in S2 cells. PNGase F treatment resulted in a band shift of the ss-Vap33 band, but not Vap33. The results were reproduced in three biologically independent experiments. Antibody to FLAG detects bands around 35 kDa, which corresponds to the molecular weight of full-length Vap33 or ss-Vap33. Antibody to α-tubulin is shown in the lower panel. Source data are provided as a Source Data file.

Western blotting. Although cytosolic GFP and nuclear FLAG-Histone H3 were not biotinylated, FLAG-Vap33-HA was prominently detected in the biotinylated fraction, indicating that Vap33 anchored on the plasma membrane exposes the MSP domain into the extracellular space (Fig. 2c). Judging from the amount of loading protein and the signal intensity of the Western blot, 10.6% of FLAG-Vap33-HA is likely to have exposed its MSP domain at the cell surface. We also examined the biotinylation status of endogenous proteins (Vap33, Tubulin, and Histone H3). To detect endogenous Vap33, we generated monoclonal antibodies against the MSP domain of Vap33 (anti-MSP^{I7145V}, anti-MSP^{I7144V}, epitope: DADLSDLNKLWKDL). The specificity of the anti-Vap33 antibodies (anti-MSP^{I7145V} and anti-MSP^{I7144V}) was validated in the *vap33* heterozygous mutant fly (*vap33*^{WT}/*vap33*^{null}), which was generated in this study (Fig. 2e). Endogenous Vap33 was clearly detected in

https://doi.org/10.1038/s41467-024-53097-5

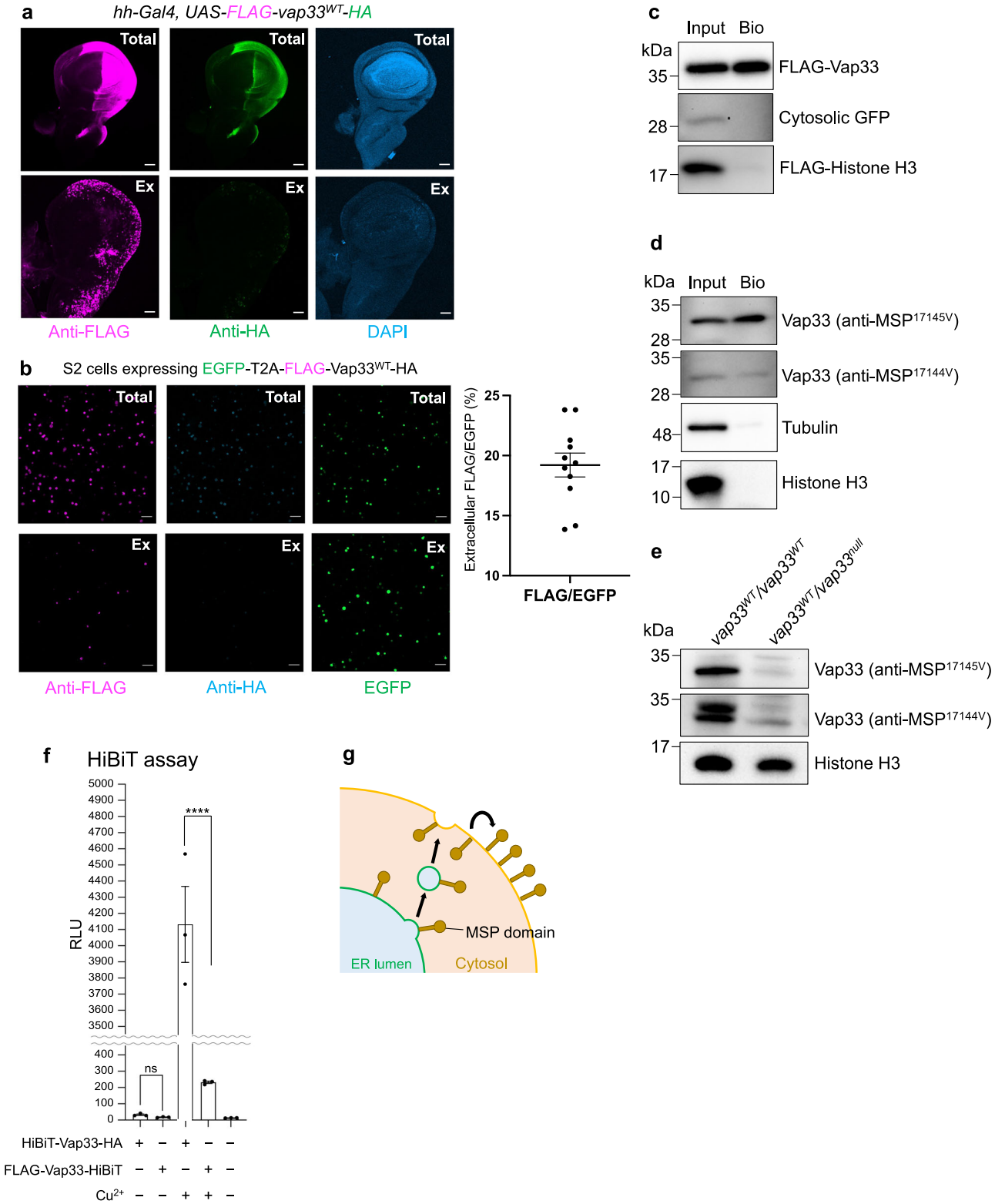

the biotinylated fraction, but cytosolic Tubulin and nuclear Histone H3 were not (Fig. 2d). These experiments further confirmed the existence of the MSP domain in the extracellular space (Fig. 2g).

We further confirmed these results by the HiBiT assay, which is a binary complementation reporter system based on luciferase activity. We fused a small HiBiT tag (11 amino acids) to the N- or C-terminus of Vap33 (HiBiT-Vap33-HA, FLAG-Vap33-HiBiT) and expressed these proteins in S2 cells using a copper-inducible expression plasmid for two days. After one day of incubation with copper sulfate ($CuSO_4$), membrane-impermeable LgBiT protein and reaction substrate were added to the cells without cell permeabilization, and the luminescence signal was then detected. With copper sulfate, the luminescence signal of HiBiT-Vap33-HA was higher than that of untransfected cells, but the luminescence signal of FLAG-Vap33-HiBiT was almost the same as that of untransfected cells (Fig. 2f). The FLAG (DYKDHDGDYKDHDI-DYKDDDDKLAAA) and HA (YPYDVPDYAGYPYDVPDYA) sequences of FLAG-Vap33^{WT}-HA have many charged amino acids, but the HiBiT sequence (VSGWRLFKKIS) has relatively few charged amino acids.

Fig. 2 | Vap33 inverts its topology on the plasma membrane, and exposes the MSP domain into extracellular space. a *Drosophila* wing disc expressing FLAG-Vap33^{WT}-HA driven by *hh-Gal4*. The results were reproduced in three biologically independent experiments. Scale bars are 40 µm. Total: total staining. Ex: extracellular staining. Magenta, green, and blue represent FLAG, HA, and DAPI, respectively. **b** S2 cells expressing EGFP-T2A-FLAG-Vap33^{WT}-HA. The results were reproduced in three biologically independent experiments. Scale bars are 50 µm. Total: total staining. Ex: extracellular staining. Magenta, blue, and green represent FLAG, HA, and fluorescence from EGFP protein, respectively. Magenta represents extracellular FLAG signal. **c**, **d** The results of cell-surface biotinylation assay. Western blotting analysis shows the biotinylated fraction (Bio) and whole cell lysate (Input) of S2 cells expressing FLAG-Vap33-HA, cytosolic GFP, and FLAG-Histone H3 (**c**), and untransfected cells (**d**). The results were reproduced in two biologically independent experiments. In the latter case, two different monoclonal antibodies generated for this study were used (see panel **e**). In **c**, 10.6% of the total FLAG-Vap33-HA is likely to expose its MSP domain at the cell surface. In **d**, based on the band intensities, 4.5% (anti-MSP^{I7144V} antibody) or 20.2% (anti-MSP^{I7145V} antibody) of the total FLAG-Vap33-HA is likely to expose its MSP domain at the cell surface. See Methods section for details. See Methods section for details. Antibodies to FLAG detect bands around 35 kDa and 17 kDa, which correspond to the molecular weight of full-length FLAG-Vap33 and FLAG-Histone H3, respectively. Antibodies to MSP, GFP, Tubulin, and Histone H3 detect bands around 30 kDa, 28 kDa, 50 kDa, and 15 kDa, respectively. **e** Validation of anti-MSP^{I7145V} and anti-MSP^{I7144V} antibodies. Lysate of wild-type and *vap33^{WT}/vap33^{null}* mutant flies were subjected to Western blotting. The results were reproduced in two biologically independent experiments. **f** HiBiT assay in S2 cells expressing HiBiT-Vap33-HA or FLAG-Vap33-HiBiT. Statistical analysis was performed by the ordinary one-way ANOVA with Dunnett's multiple comparison test (****$P < 0.0001$, ns: not significant). Error bars represent the standard error of the mean (SEM) of three biologically independent experiments ($n = 3$). **g** Schematic representation of Vap33 topology inversion. Source data are provided as a Source Data file.

Thus, the inverted topology of FLAG-Vap33^{WT}-HA is not due to artificial effects of tag insertion.

Next, to visualize the extracellularly located MSP domain, we performed an analysis using immunogold electron microscopy. The S2 cells stably expressing FLAG-Vap33-HA were stained with anti-FLAG antibody, which was labeled by gold-conjugated secondary antibody. We first confirmed the distribution of gold particles on the ER membrane (Fig. 3a, Supplementary Table 3). The gold particles on the ER membrane mostly faced the cytosol (Fig. 3a, white arrows), consistent with the split-GFP data and the *N*-glycosylation analysis (Fig. 1). In contrast, when we examined the plasma membrane, most of the gold particles localized at the extracellular face of the plasma membrane (Fig. 3b, Supplementary Table 3, and Supplementary Fig. 1, white arrows). Gold particles that were localized at the intracellular face of the plasma membrane were rarely observed (Supplementary Fig. 1, yellow arrow). These results directly demonstrate that Vap33 externalizes the MSP domain at the plasma membrane.

Given that Vap33 does not invert the topology at the ER (judged from the *N*-glycosylation status of Vap33; Figs. 1g and 3a), Vap33 topology inversion seems to occur after Vap33 protein insertion into ER membrane. To identify the subcellular site of Vap33 topology inversion, we co-expressed GFP11-Vap33-HA or FLAG-Vap33-GFP11 with Golgi-localized GFP1-10 (GFP1-10^{Golgi}; GalT::GFP1-10) or lysosome-localized GFP1-10 (GFP1-10^{Lyso}; SP::GFP1-10::LAMP1) in S2 cells. GFP1-10^{Golgi} and GFP1-10^{Lyso} were colocalized with Golgin245 and Lysotracker, indicating their proper localization at the Golgi and the lysosome (Supplementary Fig. 2a, b). The percentage of GFP^{+} cells co-expressing GFP11-Vap33-HA with GFP1-10^{Golgi} or GFP1-10^{Lyso} was significantly lower than those co-expressing FLAG-Vap33-GFP11 with GFP1-10^{Golgi} or GFP1-10^{Lyso} (Supplementary Fig. 2c, d), suggesting that Vap33 does not invert its topology at the Golgi or the lysosome membrane. Therefore, it appears most likely that the inversion event occurs at a post-Golgi membrane.

The MSP domain of uncleavable Vap33 is extracellularly localized

Although we propose that Vap33 on the plasma membrane inverts its topology, it is still possible that the extracellular FLAG-MSP signals at the plasma membrane (Fig. 2a, b and Fig. 3b) might come from cleaved MSP domain that is present in the cytosol, but not membrane-anchored Vap33. To confirm whether membrane-anchored Vap33 externalizes the MSP domain at the plasma membrane, we aimed to generate the uncleavable Vap33. The cleavage site of VAPB is predicted to lie between the MSP domain and the coiled-coil domain[15]. We generated FLAG-Vap33-HA mutants (protein isoforms, PB, PC, and PE), in which the amino acid sequences between the MSP domain and the coiled-coil domain were deleted (FLAG-Vap33$^{\Delta P115\text{-}P183}$-HA) or substituted by a GGGGGS linker sequence (FLAG-Vap33$^{\Delta P115\text{-}P183>GGGGGS}$-HA) (Supplementary Fig. 3a). We expressed these FLAG-Vap33-HAs in S2 cells, and the secreted FLAG-MSP domain in the supernatant was collected by anti-FLAG M2 magnetic beads. The collected FLAG-MSP domain was analyzed by Western blotting with anti-FLAG antibody. The cleaved MSP domain of wild-type Vap33 was detected in the supernatant, indicating that MSP domain is secreted into the cultured medium of S2 cells (Supplementary Fig. 3a). Compared with Vap33^{WT}, secretion of the MSP domain was completely inhibited in these mutant forms of Vap33 (Vap33$^{\Delta P115\text{-}P183}$ and Vap33$^{\Delta P115\text{-}P183>GGGGGS}$), suggesting that the Vap33 cleavage site is indeed located between P115 and P183. We further generated seven mutants, in which the sequence between P115 and P183 was deleted in various patterns (Vap33$^{\Delta L118\text{-}F127}$, Vap33$^{\Delta E128\text{-}T139}$, Vap33$^{\Delta S140\text{-}G150}$, Vap33$^{\Delta A151\text{-}T161}$, Vap33$^{\Delta S162\text{-}K172}$, Vap33$^{\Delta P173\text{-}S177}$, Vap33$^{\Delta E178\text{-}P183}$; Supplementary Fig. 3b). We found that the levels of MSP domain in the supernatant and whole cell lysates (WCL) were significantly reduced in Vap33$^{\Delta L118\text{-}F127}$ and Vap33$^{\Delta E128\text{-}T139}$, suggesting that these two Vap33 mutants are uncleavable (Supplementary Fig. 3b). We then expressed Vap33$^{\Delta L118\text{-}F127}$ in the wing disc and S2 cells and found a strong extracellular FLAG signal under extracellular staining conditions (Supplementary Fig. 3c,d), indicating that uncleavable Vap33 exists on the cell surface and directs its MSP domain to the extracellular space. These results indicate that membrane-anchored Vap33 is able to invert its topology at the post-Golgi membrane and exposes the MSP domain extracellularly.

The amino acid sequence in the transmembrane domain determines the topology of Vap33 on the plasma membrane

To further examine whether topology inversion is a phenomenon specific to Vap33, we compared the topology of Vap33 with other type IV integral transmembrane proteins (tail-anchored proteins: TA proteins). As control proteins, we selected four plasma membrane proteins (*CG30269, CG12012, and CG17580*), one Golgi membrane protein (*Syx13*), and one ER membrane protein (*Sec61β*) based on a previous study of *Drosophila* TA proteins[34]. FLAG and HA tags were fused to the N-termini and C-termini of these proteins, respectively. We carried out extracellular immunostaining followed by flow cytometry analysis. S2 cells transfected with these constructs were stained with anti-FLAG and anti-HA antibodies without membrane permeabilization, and analyzed by flow cytometry (Supplementary Fig. 4a, b). Upon examination of extracellular staining, the percentage of extracellular FLAG^{+} cells expressing FLAG-Vap33-HA was found to be significantly higher than that of FLAG-CG30269-HA, FLAG-CG12012-HA, FLAG-CG17580-HA, FLAG-Syx13-HA, or FLAG-Sec61β-HA (Fig. 4). These data indicates that topology inversion of Vap33 is a specific phenomenon among the type IV integral membrane proteins we investigated. However, the extracellular FLAG^{+} cells expressing FLAG-Sec61β-HA were relatively higher than those expressing FLAG-CG30269-HA, FLAG-CG12012-HA,

https://doi.org/10.1038/s41467-024-53097-5

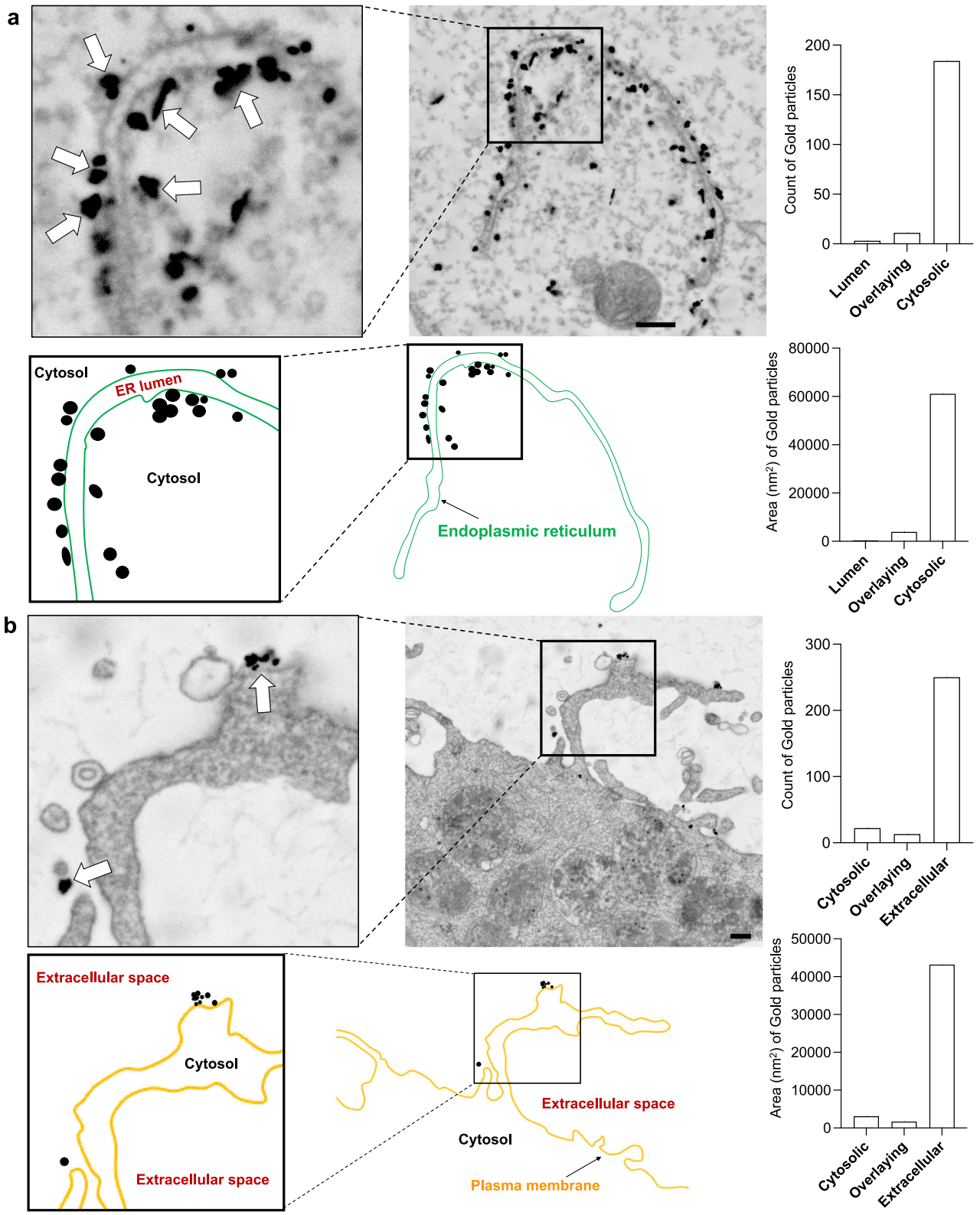

Fig. 3 | Extracellular existence of Vap33 MSP domain on the plasma membrane was demonstrated by immunoelectron microscopy analysis. a, **b** S2 cells stably expressing FLAG-Vap33^{WT}-HA were stained with anti-FLAG antibody and FluoroNanogold-conjugated secondary antibody. Stained cells were analyzed by immunoelectron microscopy. The ER (**a**) and the cell surface (**b**) are shown. Arrows in (**a**) indicate localization of the gold particles at the cytosolic face of the ER membrane, and those in (**b**) indicate localization of the gold particles at the extracellular face of the plasma membrane. Insets represent the boxed area of the right panel. Scale bars are 200 nm. Schematic representations of the microscopic images are shown. Graphs indicate the count and area (nm^2) of Gold particles. The results were reproduced in 6 biologically independent experiments for **a**, and 49 biologically independent experiments for **b**. Source data are provided as a Source Data file.

https://doi.org/10.1038/s41467-024-53097-5

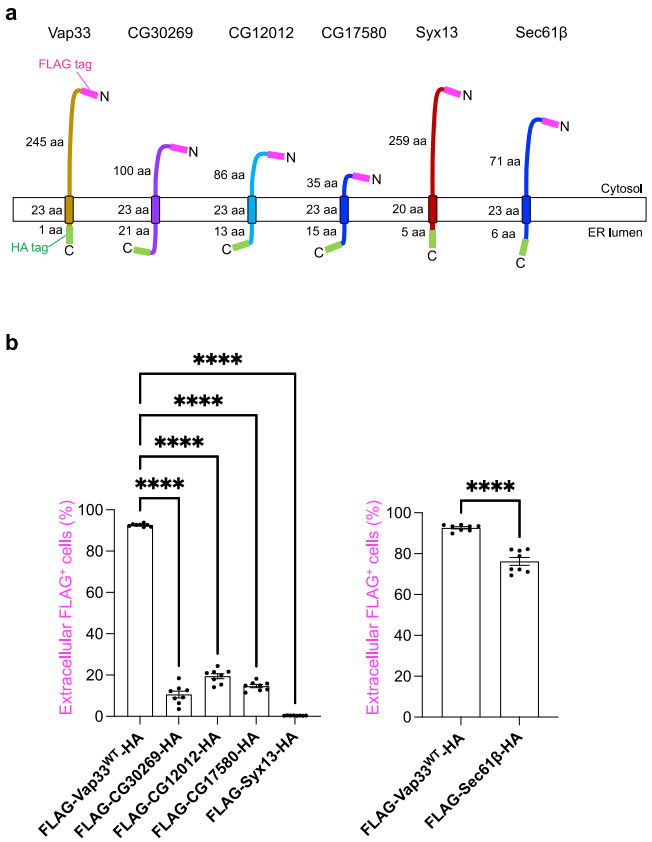

Fig. 4 | The phenomenon of topology inversion is specific to Vap33 protein among type IV integral transmembrane proteins. a Schematic diagram of type IV integral transmembrane proteins tagged with N-terminal FLAG and C-terminal HA (Vap33, CG30269, CG12012, CG17580, and Syx13). **b** Results of flow cytometry analysis of S2 cells expressing FLAG-Vap33-HA, FLAG-CG30269-HA, FLAG-CG12012-HA, FLAG-CG17580-HA, FLAG-Syx13-HA, or FLAG-Sec61β-HA. $FLAG^-HA^-$ cells were excluded from the statistical analysis. The percentage of the extracellular $FLAG^+$ cells to cells with FLAG and/or HA facing extracellularly is shown. The method for calculating the topology is explained in Supplementary Fig. 4b. Statistical analysis was performed by the ordinary one-way ANOVA with Dunnett's multiple comparison test (****$P < 0.0001$). Error bars represent the standard error of the mean (SEM) of 8 biologically independent experiments ($n = 8$). Source data are provided as a Source Data file.

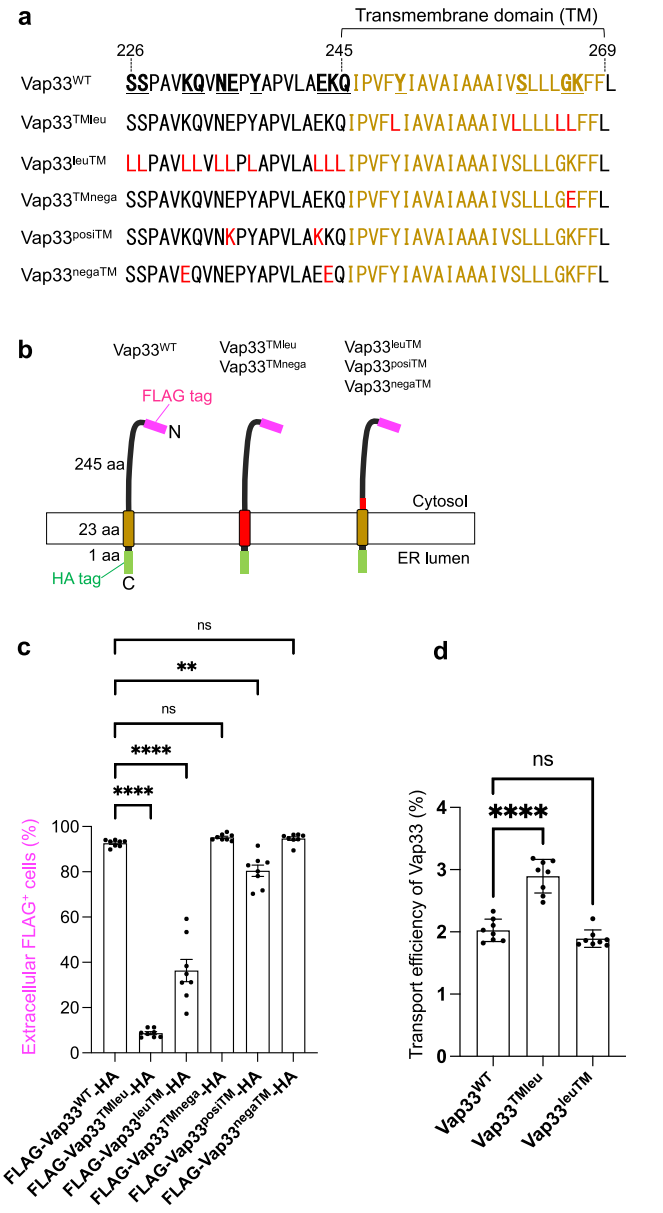

Fig. 5 | Transmembrane domain of Vap33 has an important "inversion signal". a, **b** Schematic representation of Vap33 transmembrane (TM) domain mutant constructs. **c** Results of flow cytometry analysis of S2 cells expressing FLAG-$Vap33^{WT}$-HA, FLAG-$Vap33^{TMleu}$-HA, FLAG-$Vap33^{leuTM}$-HA, FLAG-$Vap33^{TMnega}$-HA, FLAG-$Vap33^{posiTM}$-HA, or FLAG-$Vap33^{negaTM}$-HA. $FLAG^-HA^-$ cells were excluded from the statistical analysis. The percentage of the extracellular $FLAG^+$ cells to cells with FLAG and/or HA facing extracellularly is shown. Statistical analysis was performed by the ordinary one-way ANOVA (****$P < 0.0001$, **$P < 0.01$ (0.0026), ns: not significant). Error bars represent the standard error of the mean (SEM) of 8 biologically independent experiments ($n = 8$). **d** Transport efficiency of Vap33 in S2 cells expressing EGFP-T2A-FLAG-$Vap33^{WT}$-HA, EGFP-T2A-FLAG-$Vap33^{TMleu}$-HA, and EGFP-T2A-FLAG-$Vap33^{leuTM}$-HA. Transport efficiency (%) = 100 ×{(Number of $FLAG^+HA^-$ cells) + (Number of $FLAG^+HA^+$ cells) + (Number of $FLAG^-HA^+$ cells)}/(EGFP$^+$ cell number). Statistical analysis was performed by the ordinary one-way ANOVA (****$P < 0.0001$, ns: not significant). Error bars represent the standard error of the mean (SEM) of 8 biologically independent experiments ($n = 8$). Source data are provided as a Source Data file.

FLAG-CG17580-HA, or FLAG-Syx13-HA, suggesting that FLAG-Sec61β-HA also inverts the topology, although to a lesser extent than FLAG-Vap33-HA.

Previous studies have shown that polar or charged residues inside or near the transmembrane domain (TMD) are involved in topology inversion of membrane proteins[32,35,36]. Vap33 protein contains three polar amino acids (Y250, S261, and G265) and a charged amino acid (K266) in the TMD (Fig. 5a). Polar or charged amino acids are also found near the TMD. We substituted these amino acids with hydrophobic leucine, and generated Vap33 TMD mutant constructs (FLAG-$Vap33^{TMleu}$-HA, FLAG-$Vap33^{leuTM}$-HA; Fig. 5a,b). As a result of extracellular staining followed by flow cytometry analysis, we found that both FLAG-$Vap33^{TMleu}$-HA and FLAG-$Vap33^{leuTM}$-HA showed a lower extracellular $FLAG^+$ signal (Fig. 5c). The efficiency of the Vap33 transport to the plasma membrane was not decreased in FLAG-$Vap33^{TMleu}$-HA and FLAG-$Vap33^{leuTM}$-HA (Fig. 5d). Therefore, the observed decreased topology inversion of $Vap33^{TMleu}$ and $Vap33^{leuTM}$ is not due to low transport efficiency. These results suggest that topology inversion is significantly inhibited in FLAG-$Vap33^{TMleu}$-HA and $Vap33^{leuTM}$. Thus, polar or charged residues near/in the TMD are important for topology inversion.

To determine whether positive or negative charge is crucial for topology inversion of Vap33, we substituted positively charged residues (K231, K244, K266) to negatively charged Glutamate (E), and generated FLAG-$Vap33^{TMnega}$-HA and FLAG-$Vap33^{negaTM}$-HA (Fig. 5a, b). We further substituted negatively charged residues (E235, E243) to

positively charged lysine (K), and generated FLAG-Vap33^{posiTM}-HA (Fig. 5a, b). On examination of extracellular staining, the percentage of extracellular FLAG$^+$ cells expressing FLAG-Vap33^{posiTM}-HA was found to be significantly lower than that of FLAG-Vap33^{WT}-HA (Fig. 5c). Such alteration was not observed in FLAG-Vap33^{TMnega}-HA and FLAG-Vap33^{negaTM}-HA (Fig. 5c). These results suggest that negative charges near the TMD are partially required for topology inversion of Vap33, but other factors are also required to explain this phenomenon.

Investigating the involvement of the COPI/II-dependent pathway in MSP domain secretion

We examined whether Vap33 MSP domain is secreted via the conventional secretion pathway using S2 cells. dsRNA-mediated knockdown of *βCOP* (a subunit of the COPI coater complex required for retrograde vesicle transport from the Golgi to the ER) in S2 cells exhibited decreased levels of signal peptide-tagged horseradish peroxidase (ss-HRP), as reported previously[37], indicating that *βCOP* dsRNA treatment effectively inhibited the conventional secretion pathway (Supplementary Fig. 5a). We then treated S2 cells with dsRNAs against subunits of the COPI coater complex (*βCOP, γCOP*) or COPII coater complex (*Sar1, Sec13, Sec23*). After incubation for 1 day, *pUAST-attB-FLAG-Vap33^{WT}-HA* was transfected, and the secreted MSP domain was collected and analyzed by Western blotting (Fig. 6a). The proportion of secreted MSP domain to total Vap33^{WT} was 0.57% (average of N = 9 experiments). Remarkably, when we knocked-down *βCOP* and *γCOP*, the level of secreted, cleaved MSP domain was significantly decreased (Fig. 6a, the upper left panel). The knockdown of *Sar1*, *Sec13*, and *Sec23* also showed a similar effect (Fig. 6a, the lower left panel). As knockdown of *βCOP*, *γCOP*, *Sar1*, *Sec13*, and *Sec23* did not alter the expression level of Vap33, the decreased MSP secretion level by these knockdowns was not due to the decrease of Vap33 expression (Supplementary Fig. 5b).

We performed a more direct approach to test the possibility of conventional secretion of Vap33 using S2 cells stably expressing copper-inducible HiBiT-Vap33-HA (Fig. 6b). In this approach, pharmacological blockade of the Golgi-dependent transport pathway was effected by treatment with Brefeldin A (BFA), and the exposure of cell-associated MSP domain to the outside, rather than its release into the extracellular medium was assayed. In the previous report, 50 μM of BFA was added to S2 cells for blocking conventional secretion[38]. We treated the stable S2 cells with 50 μM BFA for 30 min, followed by the induction with copper sulfate. After 5 h from the induction, membrane-impermeable LgBiT protein and reaction substrate were added to the cells without cell permeabilization, and the luminescence signal was then detected. As a result, addition of BFA did not decrease the extracellular HiBiT signal, suggesting that these reagents did not inhibit the transport of Vap33 to the plasma membrane. Inhibitory effect of BFA on conventional secretion was confirmed in S2 cells expressing ss-HRP-HiBiT (Fig. 6c). These results imply that Vap33 is not secreted via the conventional secretion pathway. The inhibitory effect of COPI/II components on MSP domain secretion might be explained by their participation in a Golgi-independent transport process and/or by an indirect effect, e.g., secretion of a factor(s) required for cleavage, as investigated in the next section.

Inverted Vap33 on the plasma membrane is cleaved by extracellular proteinases Mmp1 and Mmp2

In extending the hypothesis that extracellular presentation of Vap33 MSP domain is crucial for cleavage and secretion of MSP domain, we considered it possible that Vap33 is cleaved by extracellular proteinases at the plasma membrane. ADAM metalloproteinases, a major proteinase family mediating ectodomain shedding[39], were candidates for being the proteinase(s) that cleave Vap33. To test this, we expressed FLAG-Vap33-HA together with nine different ADAM proteinases and their relatives; HA-tagged Kuzbanian-like (Kul^{HA}), HA-tagged TACE (TACE^{HA}), Mmp1, Mmp2, Meltrin, Neprilysin 3 (Nep3), HA-FLAG-tagged Goe (Goe$^{HA\text{-}FLAG}$), and CG6696[40] in S2 cells, and tested for cleavage and secretion of the MSP domain.

We found that expression of Mmp1 and Mmp2 together with FLAG-Vap33-HA significantly increased the levels of MSP domain in the supernatant, but not in WCL (Fig. 7a, quantification in Supplementary Fig. 6a). Expression of the other proteinases did not elevate the levels of secreted MSP domain (quantification in Supplementary Fig. 6a). In addition, dsRNA-mediated knockdown of endogenous Mmp1 or Mmp2 downregulated the level of secreted MSP domain (Fig. 7b). These data indicate that Mmp1 and Mmp2 are the proteinases responsible for Vap33 shedding on the plasma membrane. Furthermore, overexpression of Mmp1 or Mmp2 did not accelerate the cleavage of the uncleavable Vap33$^{\Delta L118\text{-}F127}$ (Fig. 7c), suggesting that cleavage or recognition sites for Mmp1 and Mmp2 are in L118-F127 of Vap33. We further quantified our results by flow cytometry. We transfected FLAG-Vap33-HA and Mmp1 or Mmp2 in S2 cells, and the cells were stained with anti-FLAG antibody without membrane permeabilization. The stained cells were then analyzed by flow cytometry, and the percentage of extracellular FLAG$^+$ cells was examined. Expression of Mmp1 was found to significantly reduce the extracellular FLAG signal (Fig. 7d), supporting that externalized Vap33 at the plasma membrane is cleaved by Mmp1.

Mmp1 accelerates cleavage and secretion of MSP domain of ALS8-associated mutant Vap33

It has been reported that the levels of cleavage products of the VAPB MSP domain are decreased in cerebrospinal fluid of sporadic ALS patients[18]. The MSP domain cleavage of the ALS8-associated VAPB^{P56S} mutant protein is also attenuated in primary neuronal cultures of rat[15]. In the case of *Drosophila*, P58S mutation in the Vap33 MSP domain reduced levels of the secreted MSP domain in wing disc and S2 cells[12]. We found that MSP domain cleavage and secretion were not only decreased in Vap33^{P58S}-overexpressing cells but also in cells overexpressing Vap33^{T48I}, which corresponds to the VAPB T46I mutation in ALS patients (Fig. 7e). Remarkably, overexpression of Mmp1 clearly restored the levels of secreted MSP domain derived from Vap33^{P58S} or Vap33^{T48I} (Fig. 7e). Furthermore, expression of Mmp1 significantly decreased the extracellular FLAG$^+$ signal of cells expressing FLAG-Vap33^{P58S}-HA or FLAG-Vap33^{T48I}-HA (Fig. 7f,g). These results indicate that Mmp1 can cleave ALS-associated mutant Vap33 for secretion of the MSP domain.

Discussion

In this study, we provided evidence that ER protein Vap33 inverts its topology at the post-Golgi membrane and externalizes its MSP domain at the plasma membrane, though Vap33 at the ER directs its MSP domain into cytosol (Fig. 7h). Based on its resistance to BFA treatment, the transport appears to be effected through a non-classical pathway. The inverted Vap33 is then cleaved by extracellular proteinases Mmp1 and Mmp2, and the MSP domain is released into the extracellular space. Overexpression of Mmp1 was able to increase the level of extracellular MSP domain derived from the ALS8-associated Vap33 mutants.

Cleavage and secretion of an ER-resident transmembrane protein is a largely unrecognized phenomenon. BBF2H7, which is one of the unfolded protein response (UPR)-related proteins, has also been reported to function not only at the ER membrane but also extracellularly by cleavage of the C-terminal luminal domain[41]. In response to physiological ER stress, the luminal C-terminus of BBF2H7 is processed at the transmembrane region and secreted into extracellular space. The cleaved C-terminal domain acts as a signaling molecule for cell-to-cell communication. In this study, we discovered that the ER-resident protein Vap33 could release its cytosolic domain through topology inversion. Previous studies have presented a model in which the unconventional secretion pathway provides a mechanism through

https://doi.org/10.1038/s41467-024-53097-5

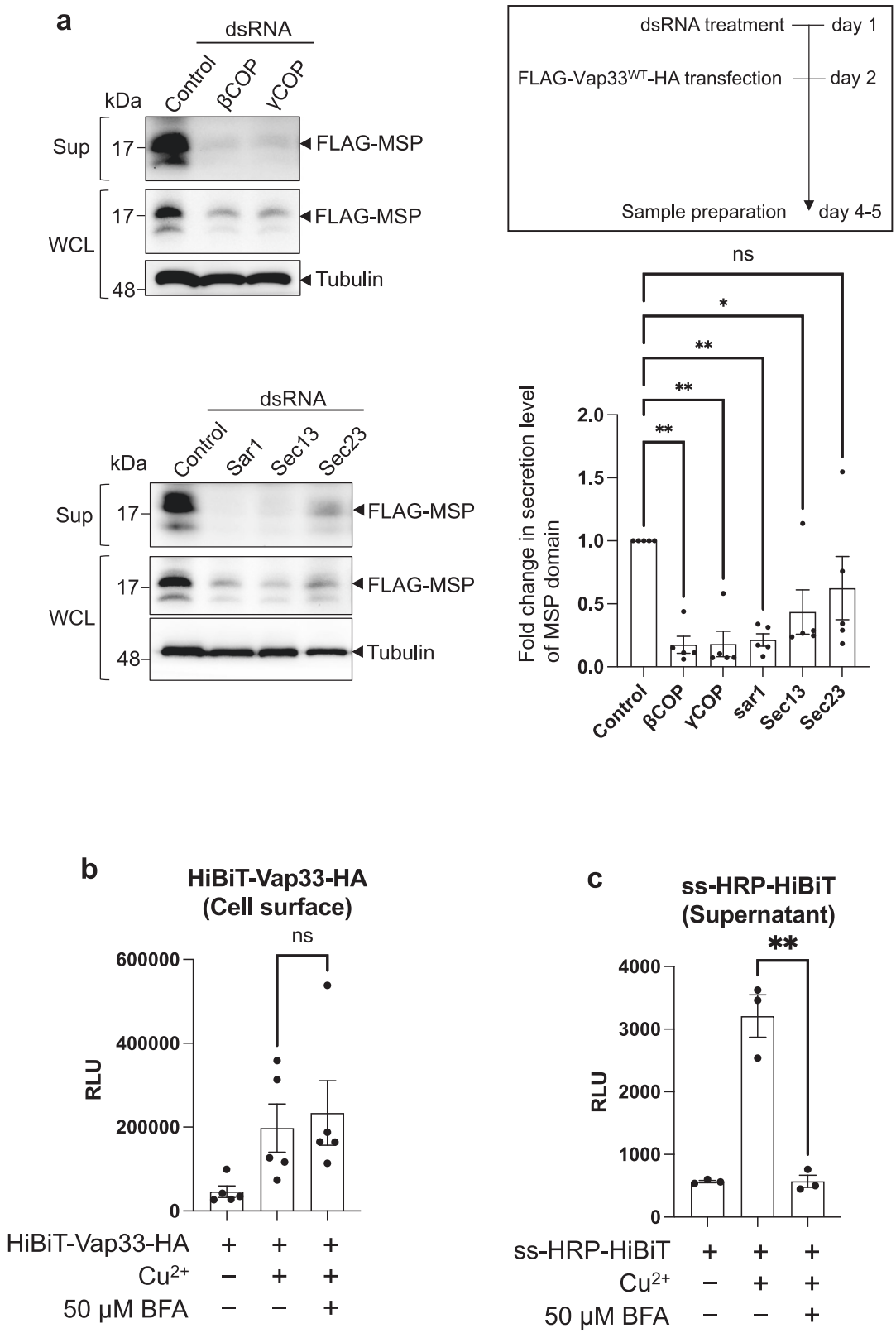

Fig. 6 | Investigating the involvement of the COPI/II dependent secretion pathway in MSP domain secretion. a Representative images of Western blot experiments of supernatant (Sup) and whole cell lysates (WCL) of dsRNA-treated S2 cells expressing FLAG-Vap33^{WT}-HA. Fold change represents ratio of the intensity of secreted MSP domain in knockdown cells to that in control cells. Antibody to FLAG detects bands around 17 kDa on a Western blot, which corresponds to the molecular weight of Vap33 MSP domain. Antibody to α-tubulin is shown below. Graphs show fold change in secretion level of MSP domain compared with Control dsRNA. Statistical analysis was performed with the ordinary one-way ANOVA (**$P < 0.01$ (*βCOP*: 0.0011, *γCOP*: 0.0012, *sar1*: 0.0019), *$P < 0.05$ (0.0293), ns: not significant). Error bars represent the standard error of the mean (SEM) of 5 biologically independent experiments ($n = 5$). **b**, **c** HiBiT assay in S2 cells expressing HiBiT-Vap33-HA (**b**) or ss-HRP-HiBiT (**c**). Statistical analysis was performed with the unpaired t-test (**$P < 0.01$ (0.0017), ns: not significant, two-sided). Error bars represent the standard error of the mean (SEM) of n biologically independent experiments ($n = 5$ for Fig. 6b, $n = 3$ for Fig. 6c). Source data are provided as a Source Data file.

https://doi.org/10.1038/s41467-024-53097-5

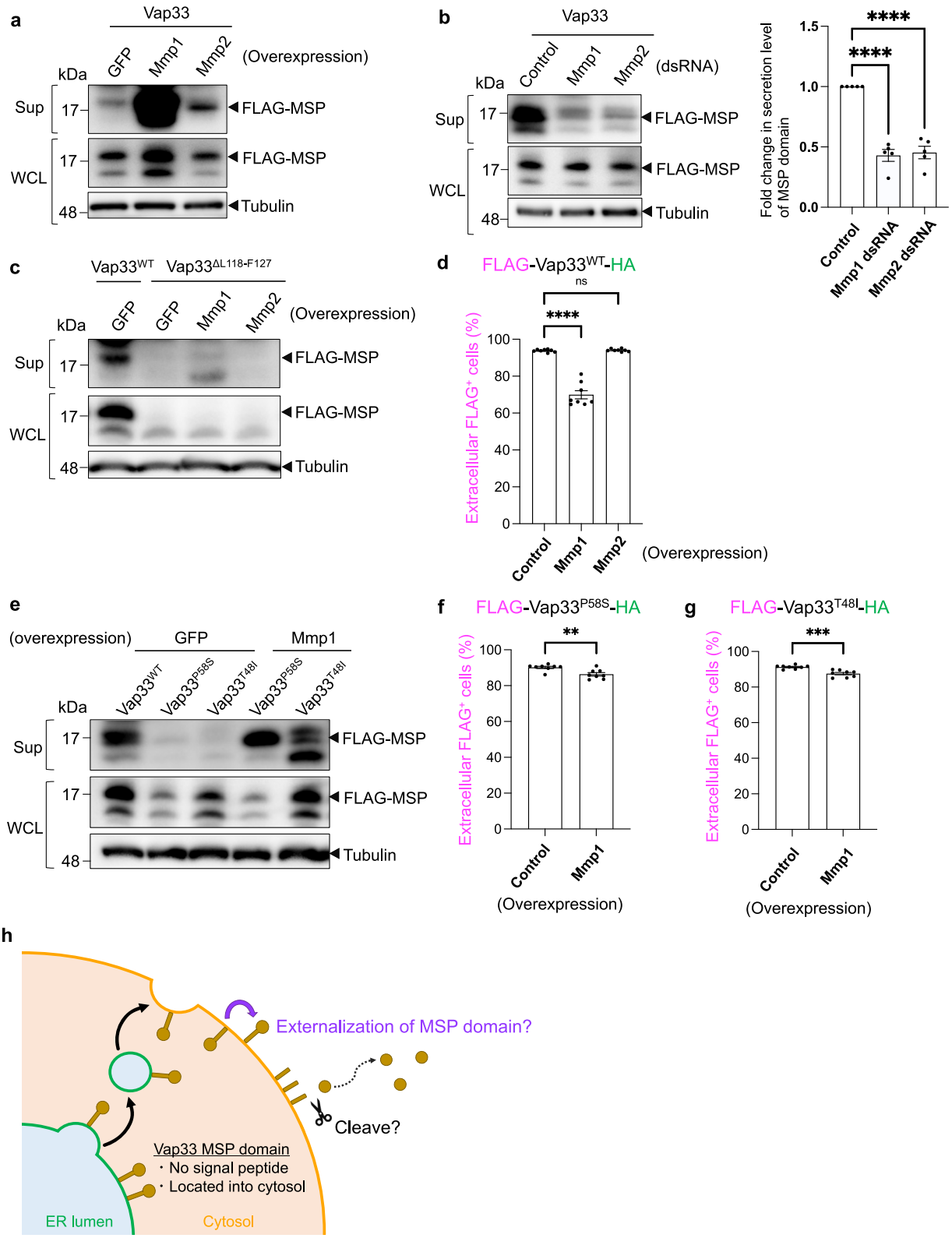

which a single protein coordinates intracellular and extracellular environments[24]. For instance, amphoterin/HMGB1 might coordinate the responses of damaged tissues by acting in the nucleus as a modulator of chromatin function, and in the extracellular space as an inducer of chemotaxis, cell motility, and inflammation[24]. Secretion of the amphoterin/HMGB1 is mediated by unconventional pathway involving exocytosis of secretory lysosomes[29].

According to our study, it is likely that Vap33 does not use the conventional secretion pathway to transport Vap33 to the plasma membrane (Fig. 6c, d), although we cannot exclude that COPI/II molecules are involved in this process (Fig. 6a). It has been reported that the Cystic Fibrosis Transmembrane conductance Regulator (CFTR) bypasses the Golgi to reach the plasma membrane by direct transport from the ER by COPII carriers[24]. The transport of Vap33

Fig. 7 | Extracellularly externalized Vap33 is cleaved by Mmp1/2 on plasma membrane. a, **c** Representative images of Western blot experiments of supernatant (Sup) and whole cell lysates (WCL) of transfected S2 cells. In Fig. 7a, FLAG-Vap33^{WT}-HA was co-expressed with GFP, Mmp1, or Mmp2. In Fig.7c, FLAG-Vap33^{WT}-HA or FLAG-Vap33$^{\Delta L118\text{-}F127}$-HA was co-expressed with GFP, Mmp1, or Mmp2. Antibody to FLAG detects bands at around 17 kDa on a Western blot, which corresponds to the molecular weight of the Vap33 MSP domain. Antibody to α-tubulin is shown below. The results were reproduced in two biologically independent experiments. **b** Representative images of Western blot experiments of supernatant (Sup) and whole cell lysates (WCL) of dsRNA-treated S2 cells expressing FLAG-Vap33^{WT}-HA. The graph shows fold change in secretion level of the MSP domain compared with control dsRNA. Statistical analysis was performed by the ordinary one-way ANOVA with Dunnett's multiple comparison test (****$P < 0.0001$). Error bars represent the standard error of the mean (SEM) of 5 biologically independent experiments ($n = 5$). **d**, **f**, **g** Results of flow cytometry analysis of transfected S2 cells stained with antibodies to FLAG and HA. The *pUASTattB* empty plasmid was used for the control. The percentage of the extracellular FLAG$^+$ cells to cells with FLAG and/or HA facing extracellularly is shown. Statistical analysis was performed by the ordinary one-way ANOVA or the unpaired t-test (****$P < 0.0001$, ***$P < 0.001$ (0.0003), **$P < 0.01$ (0.004), ns: not significant, two-sided). Error bars represent the SEM of 8 biologically independent experiments ($n = 8$). **e** Western blot experiments of supernatant (Sup) and whole cell lysates (WCL) of transfected S2 cells. Antibody to FLAG detects bands at around 17 kDa on a Western blot, which corresponds to the molecular weight of the Vap33 MSP domain. Antibody to α-tubulin is shown below. The results were reproduced in two biologically independent experiments. **h** Secretion model of Vap33. ER protein Vap33 is transported to plasma membrane via a BFA-resistant transport pathway that remains to be characterized. Vap33 inverts its topology to externalize its MSP domain. The MSP domain is then cleaved by Matrix metalloproteinase 1 and/or 2 (Mmp1/2). Source data are provided as a Source Data file.

transportation to the plasma membrane may be the same mechanism.

We found the cleaved MSP domain was present not only in the supernatant but also in the whole cell lysate (FLAG-Vap33-HA-expressing S2 cells). In addition, when the MSP domain of Vap33 was expressed in S2 cells, it was still secreted in conditioned medium[12]. Thus, there is a possibility that some MSP domain is generated in the cytosol and then secreted by an unconventional pathway. The unconventional secretion pathways appears to be induced by stress, which might impair functional integrity of the conventional secretion pathway[42]. It is possible that the MSP domain of Vap33 adopts unconventional pathways under cellular stress, such as ER stress, starvation, mechanical stress, and inflammation.

We found that the sequence between L118 and T139 is important for cleavage and secretion of Vap33. Vap33 has four isoforms (RA, RB, RC, RE), of which only Vap33-RA lacks A134-E167, which overlaps with the deleted sequence (A134-T139) of Vap33$^{\Delta E128\text{-}T139}$. Secretion of the MSP of Vap33-RA was almost completely lost (Supplementary Fig. 3e), consistent with impaired secretion of Vap33$^{\Delta E128\text{-}T139}$. *Drosophila* has only one gene (*vap33*) encoding VAP protein, whereas mammal has *VAPA* and *VAPB* as two distinct genes. Interestingly, the cleaved MSP domain of VAPB in forebrain and cerebellum was reported to be higher than that of VAPA[14]. The cleavage efficiency of splicing isoforms of Vap33, Vap33-RA and Vap33-RB/RC/RE are reminiscent of mammalian VAPA and VAPB, respectively. It is speculated that Vap33-RA has specialized for organelle tethering function, but Vap33-RB/RC/RE have come to play roles in both intra- and extracellular environments.

In this study, we found the topology inversion of the ER-resident transmembrane protein Vap33. Syntaxin-2, the other type IV transmembrane protein, was also reported to invert the topology in human pancreatic β-cells[43]. The mechanism underlying this event seems to differ among various cell types. In bacterial cells and human pancreatic β-cells, the reversal of topology occurs after membrane insertion[31,43], whereas it occurs during protein synthesis (membrane translocation) at the ER membrane in human lung cells[32]. It is typically assumed that inversion of a membrane protein after membrane insertion is thermodynamically more difficult than during membrane insertion. According to our data (split-GFP experiments and *N*-glycosylation assay), the reversal of Vap33 topology does not occur at the ER membrane, supporting the hypothesis that inversion event of Vap33 occurs in a post-insertional manner.

We showed that the sequence in the TMD has an important "inversion signal". Our results suggest that negatively charged residues are particularly required for the inversion. This is consistent with previous studies showing that negatively charged residues appear to affect topology when they are present in high numbers[44], or when they lie within seven flanking residues from the end of the hydrophobic TMD[45]. The transmembrane domain of Vap33 contains three polar amino acids and one charged amino acid (Fig. 5a). Syntaxin-2 also has three polar amino acids but no charged amino acid[33]. Thus, Vap33 and Syntaxin-2 may adopt partially similar mechanism to invert the topology. However, the precise mechanism governing the inversion remains to be fully elucidated. Changes in the levels of specific lipids (e.g., ceramide, phosphatidylethanolamine) have been reported to invert the topology of membrane proteins before or after membrane insertion[32,35,36]. The ATAD1/Msp1 complex is an AAA-ATPase and acts as a membrane extractor (dislocase) when non-mitochondrial proteins are misinserted into the mitochondrial membrane[46]. The extracted TA proteins are then reinserted into their respective target membrane or are degraded via ER-associated degradation (ERAD). The ATP-driven extraction system gives mislocalized TA proteins a second chance to target their correct location. An analogous membrane extractor at the ER is the P-type ATPase P5a-ATPase, which recognizes and translocates non-ER TA proteins[46,47]. We propose that such a membrane extractor also serves to invert the topology of membrane proteins. Given that Vap33 is an ER-resident protein, the presence of Vap33 at the post-Golgi membrane could be recognized as an abnormal state and promote the interaction of Vap33 with the dislocase, which extracts the cell surface Vap33 and Vap33 could be reinserted as an inverted topology. The topology inversion we observed here could be an "extraction and reinsertion event". However, the precise mechanism responsible for the inversion and the generality of the phenomenon are poorly understood.

The mechanism by which cytosolic proteins are secreted to extracellular space has remained a riddle. A variety of secretion pathway have been proposed, and these are categorized as unconventional secretion pathways[24,42,48]. If the phenomenon of topology inversion occurs in multiple membrane proteins, cytosolic part of those transmembrane proteins might be secreted via the ER to Golgi-dependent conventional secretion pathway accompanied by topology inversion. Therefore, investigating the molecular mechanism underlying topology inversion might lead to an understanding of unconventional secretory pathways.

We succeeded in identifying proteinases responsible for cleaving Vap33. Overexpression of Mmp1 and Mmp2 significantly promoted secretion of the MSP domain. In the case of Mmp1, the effect on MSP domain secretion was drastic: secretion levels became 20-fold higher than the control (Supplementary Fig. 6). Although 23 different MMPs have been recognized in human, *Drosophila* has only two MMPs; dMMP1 and dMMP2, which are orthologous to human MMP14/24 and MMP15, respectively (FlyBase data). Human MMPs (MMP1, MMP2, MMP3, and MMP9) in serum have been reported to be associated with ALS[49,50]. Given that the MSP domain of VAPB is reduced in sporadic ALS patients[18], accelerating MSP domain secretion by activating MMPs in ALS patients might be a therapeutic strategy of ALS disease. However, elevating MMPs in neuronal tissue could harm the physiological integrity of neurons because MMPs are well known to degrade extracellular matrix (ECM) to remodel a wide range of ECM components

during brain development[49]. The actions of MMPs are crucial for maintaining brain physiology. In fact, overexpression of dMMP1 specifically in motor neurons rather induced ALS-like phenotypes such as motor deficits[49]. Furthermore, substrates of MMPs are known to be promiscuous[51], and overexpression of MMPs will provoke multiple side effects. Alternatively, enhancing the topological inversion of Vap33 in motor neurons might be a more desirable way to promote MSP domain secretion because it does not require overexpression of MMPs. A deeper understanding of the mechanisms regulating Vap33 topology will be required to establish this therapeutic strategy.

Methods

Fly strains

The fly genotypes used in this study are as follows: *y w;; Actin-Gal4/TM6B Tb* (BDSC38461). *w;; hh-Gal4/TM6B Tb* (kindly gifted from Masayuki Miura, The Univ of Tokyo). *C164-Gal4* (BDSC 33807). *UAS-attB-FLAG-Vap33^{WT}-HA/CyO* and *UAS-attB-FLAG-Vap33$^{\Delta L118\text{-}F127}$-HA/CyO* were generated in this study. These flies were maintained at 18–25 °C (standard laboratory conditions).

Immunohistochemistry of fly wing disc

Immunostaining of fly wing discs was conducted according to the following protocol. For total staining, wing discs of third instar larvae were dissected in PBST [phosphate-buffered saline (PBS) containing 0.3% Triton X-100], and fixed in 4% paraformaldehyde (PFA) for 20 min at room temperature. Fixed discs were washed three times for 20 min at room temperature and were blocked in 5% normal goat serum in PBST for 1 h at room temperature. The discs were incubated in PBST containing primary antibodies overnight at 4 °C. After being washed three times with PBST for 20 min, discs were incubated with secondary antibodies in PBST in the dark for 2 h at room temperature. After washing discs three times for 20 min, discs were mounted with SlowFade (Invitrogen, S36972). For extracellular staining, wing discs were dissected in ice-cold Schneider's Insect Medium (Sigma, S0146). The discs were incubated in ice-cold Schneider's Insect Medium containing primary antibodies for 30 min. The discs were then washed three times with ice-cold PBS for 20 min and fixed in 4% PFA for 20 min on ice. After being washed three times with ice-cold PBS for 20 min, discs were incubated overnight in the dark with secondary antibodies and DAPI (0.15 µg/ml, Nacalai Tesque, 11034-56) in PBS at 4 °C. After being washed three times for 20 min, discs were mounted with SlowFade. Images were acquired by laser-scanning confocal microscope (Zeiss LSM Pascal or Zeiss LSM900). The following primary antibodies were used: mouse anti-FLAG M2 (1:200 for total staining and 1:50 for extracellular staining, Sigma, F1804) and rat anti-HA 3F10 (1:200 for total staining and 1:40 for extracellular staining, Sigma, 11867423001). The following secondary antibodies were used: goat anti-rat IgG Alexa 568 (1:250, Invitrogen, A11077) and goat anti-mouse IgG Alexa 488 (1:250, Invitrogen, A11029).

DNA construction

To generate the *pUAST-attB-FLAG-Vap33^{WT}-HA* plasmid, we obtained *FLAG-Vap33^{WT}-HA* cDNA from a transgenic fly possessing *UAS-FLAG-Vap33^{WT}-HA* (kindly gifted from Hugo Bellen, Baylor College of Medicine). The *FLAG-Vap33^{WT}-HA* fragment was amplified from the fly extract, and subcloned into the *pUAST-attB* vector. The mutant forms of *pUAST-attB-FLAG-Vap33^{WT}-HA* (*vap33$^{\Delta P115\text{-}P183}$*, *vap33$^{\Delta L118\text{-}F127}$*, *vap33$^{\Delta E128\text{-}T139}$*, *vap33$^{\Delta S140\text{-}G150}$*, *vap33$^{\Delta A151\text{-}T161}$*, *vap33$^{\Delta S162\text{-}K172}$*, *vap33$^{\Delta P173\text{-}S177}$*, *vap33$^{\Delta E178\text{-}P183}$*, *ss-vap33*, *vap33^{TMleu}*, *vap33^{leuTM}*, *vap33^{TMnega}*, *vap33^{posiTM}*, *vap33^{negaTM}*, *vap33^{P58S}*, *vap33^{T48I}*) and *pUAST-attB-FLAG-vap33-RA-HA* were generated using PrimeStar (Takara, R045A), KOD One (TOYOBO, KMM-101), In-Fusion (Takara, 639648), Ligation high Ver.2 (TOYOBO, LGK-271), and NEBuilder HiFi DNA Assembly Master Mix (New England Biolabs, E2621). To construct *vap33$^{\Delta P115\text{-}P183>GGGGGS}$*, we obtained the GGGGGS repeated linker sequence from Eurofins. The linker sequence was amplified using PrimeStar, and subcloned into *pUAST-attB-FLAG-Vap33^{WT}-HA* using In-Fusion. For generating *pMT-ss-HRP-FLAG*, *pMT-ss-HRP* was amplified from an *ss-HRP-V5-His* plasmid[37] using PrimeStar, and FLAG sequence was subcloned into the linearized vector using NEBuilder. To generate *pUAST-attB-GFP11×7-Vap33-HA* and *pUAST-attB-FLAG-Vap33-GFP11×7*, the GFP11×7 sequence[28] was amplified using PrimeStar, and subcloned into the *pUAST-attB-FLAG-Vap33^{WT}-HA* using Ligation high Ver.2. For *pUAST-attB-ss-FLAG-GFP11×7-Vap33-HA* and *pUAST-attB-ss-FLAG-Vap33-HA*, signal peptide sequence derived from the *ss-HRP-V5-His* plasmid was subcloned into *pUAST-attB-GFP11×7-Vap33-HA* and *pUAST-attB-FLAG-Vap33-HA* using NEBuilder. *pACUH-GFP1-10* (GFP1-10^{Cyto}) and *pACUH-SP-GFP1-10-SEHDEL* (GFP1-10ER)[28]. To generate *pAc5-STABLE-FLAG-Vap33^{WT}-HA-T2A-Neo^{R}*, *pAc5-STABLE-T2A-Neo^{R}* was amplified from *Ac5-STABLE2-neo* plasmid (Addgene#32426) using KOD One, and the FLAG-Vap33^{WT}-HA fragment was subcloned into the linearized vector using NEBuilder. To generate *pMT-HiBiT-Vap33-HA* or *pMT-FLAG-Vap33-HiBiT*, we amplified *FLAG-Vap33* or *Vap33-HA* sequence from *pUAST-attB-FLAG-Vap33^{WT}-HA* plasmid using KOD one. The *FLAG-Vap33* (or *Vap33-HA*) and *HiBiT* sequence was subcloned into *pMT-puro* (addgene#17923) plasmid using NEBuilder. To generate *pMT-ss-HRP-HiBiT*, the *HiBiT* sequence was subcloned into *pMT-ss-HRP* vector amplified from the *pMT-ss-HRP-FLAG* plasmid. To generate *pUAST-attB-EGFP-T2A-FLAG-Vap33^{WT}-HA*, EGFP-T2A fragment was amplified from *Ac5-STABLE2-neo* plasmid (Addgene#32426) using KOD One and was subcloned into *pUAST-attB-FLAG-Vap33^{WT}-HA* plasmid. To generate *pUAST-attB-EGFP-T2A-FLAG-Vap33^{TMleu}-HA and pUAST-attB-EGFP-T2A-FLAG-Vap33^{leuTM}-HA*, *FLAG-Vap33^{TMleu}-HA or FLAG-Vap33^{leuTM}-HA* fragment was amplified from *pUAST-attB-FLAG-Vap33^{TMleu}-HA or pUAST-attB-FLAG-Vap33^{leuTM}-HA* plasmid and was subcloned into *pUAST-attB-EGFP-T2A* vector. To generate *pUAST-attB-FLAG-CG30269-HA*, *pUAST-attB-FLAG-CG12012-HA*, *pUAST-attB-FLAG-CG17580-HA*, *pUAST-attB-FLAG-Syx13-HA*, and *pUAST-attB-FLAG-Sec61β-HA*, we obtained plasmids containing cDNA from the *Drosophila* Genomics Resource Center (DGRC) (FMO10055: DGRC Stock 1637586, UFO11313: DGRC Stock 1641315, UFO08616: DGRC Stock 1642791, FMO07283: DGRC Stock 1620738, FMO12676: DGRC stock 8298). The *CG30269, CG12012, CG17580, Syx13*, and *Sec61β* cDNA fragment were amplified from each plasmid using KOD One, and subcloned into the *pUAST-attB* vector (which includes an N-terminal FLAG-tag and a C-terminal HA-tag) using NEBuilder. For constructing *pUAST-attB-GalT::GFP1-10* (GFP1-10^{Golgi}) or *pUAST-attB-SP::GFP1-10::LAMP1* (GFP1-10^{Lyso}), the GalT and LAMP1 sequence (derived from plasmids kindly gifted from Akiko Satoh; Addgene #36205 and #34831) and the GFP1-10 sequence[28] was amplified using KOD One, and subcloned into the *pUAST-attB* vector using NEBuilder. For constructing *pUAST-attB-GalT::GFP11×7* (GFP11^{Golgi}) or *pUAST-attB-SP::GFP11×7::LAMP1* (GFP11^{Lyso}), the *GFP11×7* sequence was amplified from *pUAST-attB-GFP11×7-Vap33-HA* using KOD One, and subcloned into the *pUAST-attB-GalT* or *pUAST-attB-SP::LAMP1* vector using NEBuilder. *UAS*-expression plasmids including Kul^{HA}, TACE^{HA}, Mmp1, Mmp2, Meltrin, Nep3, Goe$^{HA\text{-}FLAG}$, and CG6696 were gifted from Petri et al.[40]. The primers used to generate these constructs are available in Supplementary Table 4.

Cell culture and transfection

S2 cells (kindly gifted from Akiko Satoh) were grown at 25 °C in Schneider's *Drosophila* Medium (1×, Gibco, 21720) supplemented with 10% heat-inactivated Fetal Bovine Serum (Biological Industries, 04-007-1 A) with 100 units/ml penicillin and 100 µg/ml streptomycin (Wako, 168-23191). Cells were transfected using the Effectene Transfection Reagent (Qiagen, 301425) according to the manufacturer's instructions. We used *Actin-Gal4* as a driver for each *UAS* transgene (*Actin-Gal4*: *UAS* ratio is 2:1). Plasmids (1.8 µg, 0.6 µg, 0.3 µg, and 0.15 µg) were transfected in the S2 cells seeded on a 6 cm dish, a 6-well plate, a 12-well-plate, and a 24-well plate, respectively.

Generation of anti-MSP antibodies

Monoclonal antibodies against the MSP domain of Vap33 (anti-MSP^{17145V}, anti-MSP^{17144V}, epitope: DADLSDLNKLWKDL) were generated by Europhins.

Preparing supernatant and WCL fraction for western blotting analysis

To prepare a supernatant fraction from the S2 cells, the cells were seeded on plates (6.0×10^6 cells/6 cm dish for FLAG-Vap33-HA expression and 3.0×10^6 cells/well in a 6-well plate for ss-HRP-FLAG expression) and transfected with plasmids to express the indicated proteins. For ss-HRP-FLAG expression, $CuSO_4$ was added to the medium at a final concentration of 500 µM, 1 day before sample preparation. After growing the cells for 4–5 d, the medium was centrifuged at 2000–5000 rpm for 5 min to remove cells, and filtered with a 0.20 µm membrane filter (Advantec, 25CS0202AS). The medium was then incubated with anti-FLAG M2 Magnetic Beads (Sigma, M8823) for 1–3 h at 25 °C. The bound materials were washed twice with buffer TBS (50 mM Tris HCl, 150 mM NaCl, pH 7.4), and eluted in 20 µl of sample buffer without dithiothreitol (80 mM Tris-HCl (pH 6.8), 2% SDS, 15% glycerol, brilliant blue). After being boiled for 5 min, the eluted proteins were mixed with 5× sample buffer containing dithiothreitol (200 mM Tris-HCl (pH 6.8), 250 mM dithiothreitol, 5% SDS, 36.5% glycerol, bromophenol blue), and were subjected to SDS-PAGE and immunoblotting.

For preparation of the WCL, after growth, the cells were collected by centrifugation and added to 2% SDS/PBS. After sonication and measurement of protein concentration, the lysates were mixed with the 5× sample buffer. The samples were then boiled for 2 min and subjected to SDS-PAGE and immunoblotting.

For preparation of fly lysates, 20 flies were washed in PBS, and homogenized in 50 µl of PBST on ice. After adding 50 µl of 2% SDS/PBS, the lysates were subjected to sonication, centrifuged for 12,000 g for 10 min at 4 °C, and the supernatant was collected. After measurement of protein concentration, the lysates were mixed with the 5× sample buffer. The samples were then boiled for 5 min and subjected to SDS-PAGE and immunoblotting.

dsRNA treatment

Templates for dsRNA transcription were generated by PCR amplification of target gene sequences using 5′ and 3′ primers corresponding to target sequences and the T7 promoter (5′-TAATACGACTCACTA-TAGGG-3′). *pBluescript SK* plasmid[52] or genome DNA extracted from *Drosophila melanogaster* was used for the PCR templates. We used dsRNA targeting *pBluescript SK* as a control dsRNA. Except for *pBluescript* and *βCOP*, target sequences for dsRNA were determined by UP-TORR[53]. Primer sequences are listed in Supplementary Table 5. In vitro transcription was carried out using the T7 RiboMAX Express RNAi System (Promega, P1700) according to the manufacturer's protocol. The S2 cells expressing FLAG-Vap33-HA (in a 6 cm dish) and those expressing ss-HRP-FLAG (in a 35 mm dish) were treated with 50 µg and 20 µg dsRNA, respectively. The dsRNA treatment was performed in Express Five Serum Free Medium (1×, Gibco, 10486-025). After incubation for 1 h at 25 °C, the Schneider's *Drosophila* Medium (supplemented with 10% heat-inactivated Fetal Bovine Serum and penicillin/streptomycin) was added to the dsRNA-treated cells, which were allowed to grow for 1 d at 25 °C. The cells were then transfected with *pUAST-attB-FLAG-Vap33^{WT}-HA* or *pMT-ss-HRP-FLAG* plasmid. After 4–5 d, the supernatant and WCL were prepared as described above.

PNGase F treatment

To detect *N*-glycosylation, we used a PNGase F kit (New England Biolabs, P0704S). Cells (2.0×10^6 cells/well) in Schneider's *Drosophila* Medium (supplemented with 10% heat-inactivated Fetal Bovine Serum and penicillin/streptomycin) were seeded on 6-well plates and transfected with FLAG-Vap33-HA or ss-FLAG-Vap33-HA. After incubation for 3 d at 25 °C, the cells that had grown were collected by centrifugation and resuspended in Glycoprotein Denaturing Buffer. After sonication and boiling for 10 min, the protein concentration of the cell lysates was measured, and 40 µg protein was mixed with 10× GlycoBuffer2 (New England Biolabs, B3704S), 10% NP-40 (New England Biolabs, B2704S), H_2O, and PNGase F according to the manufacturer's protocol. After incubation overnight at 37°C, the treated cell lysates were supplemented with 5× sample buffer and subjected to SDS-PAGE and immunoblotting.

Cell surface biotinylation assay

For the cell surface biotinylation assay, 2.0×10^6 cells/well in Schneider's *Drosophila* Medium (supplemented with 10% heat-inactivated Fetal Bovine Serum and penicillin/streptomycin) were seeded on 12-well plates and transfected with the indicated plasmids. After 3 d growth at 25 °C, the cells were washed three times with PBS and incubated with 0.5 mg/ml EZ-Link Sulfo-NHS-LC-Biotin (ThermoFisher Scientific, 21335) in PBS for 30 min on ice. The biotinylation reaction was stopped with 50 mM NH_4Cl in PBS. After stopping the reaction, the cells were eluted in 2% SDS/PBS for 30 min at room temperature. The cells were then subjected to sonication and incubated with 50% Streptavidin Sepharose High Performance (GE Healthcare, 17-5113-01) in PBS overnight at room temperature. After being washed out from the Streptavidin beads with 2% SDS/PBS, the protein solutions were supplemented with 5× sample buffer, boiled for 3 min. 30 µl of cell lysates and total amount of the biotinylated fraction was then subjected to SDS-PAGE and immunoblotting. In Fig. 2c, the input was 30 µg protein from 311 µg cell lysate used for the streptavidin pulldown, and the ratio of band intensity of Biotinylated fraction to Input is 1.1. Thus, 10.6% of the total FLAG-Vap33-HA is likely to expose its MSP domain at the cell surface. For immunoblotting using anti-MSP^{17145V} antibody in Fig. 2d, the input was 30 µg protein from 223 µg cell lysate used for the streptavidin pulldown, and the ratio of band intensity of Biotinylated fraction to Input is 1.5. For immunoblotting using anti-MSP^{17144V} antibody in Fig. 2d, the input was 30 µg protein from 232 µg cell lysate used for the streptavidin pulldown, and the ratio of band intensity of Biotinylated fraction to Input is 0.35. Thus, 4.5–20.2% of the total FLAG-Vap33-HA is likely to expose its MSP domain extracellularly.

The three estimates of exposed MSP domain against total Vap33 (10.6%, 4.5%, 20.2%) is qualitatively similar.

Western blot analysis

Total volume of eluted proteins from supernatant and 30 µg of cell lysates were subjected to SDS-PAGE analysis (15% polyacrylamide gel for Vap33, MSP domain, ss-HRP, Tubulin, Histone H3, and GFP detection; 10% polyacrylamide gel for ss-Vap33 and Tubulin detection) and immunoblotting. Proteins subjected to SDS-PAGE were transferred to Immobilon-PSQ PVDF membrane (0.2 µm pore size, Millipore, ISEQ00010). Mouse monoclonal antibody to FLAG (1:2000-1:1000, Sigma, F1804), rabbit polyclonal antibody to FLAG (1:1000, Sigma, F7425), rabbit monoclonal antibody to Vap33 MSP domain (1:4000-1:2000, 17144 V/17145 V), mouse monoclonal antibody to human α-tubulin (1:2000, Cedarlane, CLT9002), mouse monoclonal antibody to Histone H3 (1:4000-1:2000, Active Motif, 39064), and rabbit polyclonal antibody to GFP (1:2000, Invitrogen, A6455) were used as primary antibodies. Horseradish peroxidase-conjugated antibody to mouse IgG (1:20000, Jackson ImmunoResearch, 715-035-150) and to rabbit IgG (1:40000–1:10000, Jackson ImmunoResearch, 715-035-152) were used as secondary antibodies. Pierce ECL-plus Western Blotting Substrate (Thermo Scientific, 32132) and ChemiDoc Touch MP (Bio-Rad) were used for detection. The intensities of bands were quantified using Image Lab. Uncropped scans of all the blots were supplied in the Source Data and Supplementary Fig. 7-11.

Flow cytometry analysis

For detecting topology of membrane proteins in S2 cells, fluorescence-activated cell sorting (flow cytometry) analysis was performed. Cells (5×10^5 cells/well) in Schneider's *Drosophila* Medium (supplemented with 10% heat-inactivated Fetal Bovine Serum and penicillin/streptomycin) were seeded on 24-well plates, and transfected with the indicated plasmids. After incubation for 3 d at 25 °C, the cells in each well were transferred into tubes, and centrifuged at 300 g for 5 min at 4 °C. After removal of the culture medium, the cells were incubated in PBS (supplemented with 0.1% BSA and 0.1% NaN_3) for 30 min on ice. For detection of topology at the plasma membrane, the cells were then treated with APC-conjugated antibody to FLAG (1:1000-1:500, BioLegend, 637307) and PE-conjugated antibody to HA (1:1000-1:500, BioLegend, 901517) in the dark for 20 min on ice. The treated cells were washed in ice-cold PBS (supplemented with 0.1% BSA and 0.1% NaN_3), and fixed with 4% PFA for 20 min at room temperature. After washing out in PBS, the cells were subjected to flow cytometry analysis using a Sony MA900 flow cytometry machine, guided by gates established by untransfected cells stained in parallel (for detecting $FLAG^+$ and/or HA^+ cells). When comparing GFP^+ cells in Fig. 1C, F, S3C, and S3D, we used the percentage of the cells whose GFP signals were above the indicated lines of the histograms.

Immunocytochemistry of S2 cells

For the immunocytochemistry shown in Fig. 1, the transfected S2 cells were fixed with 4% PFA, and mounted with SlowFade. For total staining in Fig. 2b and Supplementary Fig. 3d, transfected cells were fixed in 4% PFA containing 0.5% Triton X-100 for 20 min at room temperature. The cells were blocked with PBS (supplemented with 0.1% BSA and 0.1% NaN_3) for 1 h at room temperature, and incubated in PBS (supplemented with 0.1% BSA and 0.1% NaN_3) containing primary antibodies for 1 h at room temperature. After being washed three times, cells were incubated with secondary antibodies and 0.2 μg/ml DAPI in PBS (supplemented with 0.1% BSA and 0.1% NaN_3) in the dark for 1 h at room temperature. After washing cells three times, cells were mounted with SlowFade. For extracellular staining in Fig. 2b and Supplementary Fig. 3d, transfected cells were blocked with PBS (supplemented with 0.1% BSA and 0.1% NaN_3) for 30 min on ice, and incubated in PBS (supplemented with 0.1% BSA and 0.1% NaN_3) containing primary antibodies for 1 h on ice. After being washed three times, cells were incubated with secondary antibodies in PBS (supplemented with 0.1% BSA and 0.1% NaN_3) in the dark for 1 h on ice. After washing cells three times, cells were fixed in 4% PFA for 20 min at room temperature and were mounted on slide glass with SlowFade. The following primary antibodies were used: mouse anti-FLAG M2 (1:1000 for total staining and 1:100 for extracellular staining, Sigma, F1804) and rat anti-HA 3F10 (1:200 for total staining and 1:20 for extracellular staining, Sigma, 11867423001). The following secondary antibodies were used: goat anti-rat IgG Alexa 568 (1:250, Invitrogen, A11077), goat anti-mouse IgG Alexa 555 (1:250, Invitrogen, A32727), goat anti-mouse IgG Alexa 488 (1:250, Invitrogen, A11029), and goat anti-mouse IgG Alexa 633 (1:250, Invitrogen, A21052). For immunolabeling Golgi apparatus in Supplementary Fig. 2a, the S2 cells transfected with the indicated proteins were cultured for 3 d. The cells were seeded on a cover slip, added with concanavalin A solution (0.5 mg/ml), and then fixed in 4% PFA (0.5% Triton X-100) for 20 min at room temperature. After washing out in PBS (0.1% BSA, 0.1% NaN_3), the cells were incubated with goat polyclonal antibody to *Drosophila* Golgin-245 (1:500, DSHB) for 1 h at room temperature. After washing out, the cells were further incubated with Alexa Fluor 568 donkey anti-goat IgG (1:250, Molecular Probes, A11057) in the dark for 1 h at room temperature. After washing out, the stained cells were mounted with SlowFade. For labeling lysosomes in Supplementary Fig. 2b, the transfected S2 cells were treated with LysoTracker Red DND-99 (1:50, Thermo Scientific, L7528). The treated cells were then fixed and mounted as described above.

HiBiT assay

For HiBiT assay in Fig. 2g and Fig. 6c, d, we used Nano-Glo HiBiT Extracellular Detection System (Promega, N2420). For Fig. 2h, S2 cells (1.5×10^6 cells/well) were seeded on a 12-well plate, transfected with the indicated plasmid. After 2 days, the cells were incubated with 0.2 mM $CuSO_4$(II) for 20 h. 60 μl of cell suspension (2×10^6 cells/ml) was mixed with 30 μl of Extracellular reagent (0.3 μl of LgBiT protein + 0.6 μl of HiBiT Extracellular substrate + 30 μl of HiBiT Extracellular buffer) and the cell suspension was spread in a 96-well plate. After incubating for 5 min at room temperature, HiBiT signal was detected by SpectraMax iD3 plate reader (Molecular devices). For Fig. 6c, S2 cells stably expressing HiBiT-Vap33-HA (2×10^5 cells/well) were seeded on a 96-well plate. After 24 h, 100% EtOH or 50 μM BFA (diluted in 100% EtOH) was added and incubated for 30 min. The cells were then treated with 0.5 mM $CuSO_4$(II) for 5 h. After washed with PBS twice, HiBiT signal was detected as described above. For Fig. 6d, S2 cells (2×10^5 cells/well) were seeded on a 96-well plate, and transfected with ss-HRP-HiBiT. After 24 h, 100% EtOH or 50 μM BFA (diluted in 100% EtOH) was added and incubated for 30 min. The cells were then treated with 0.5 mM $CuSO_4$(II) for 5 h. The supernatant was mixed with 50 μl of Extracellular reagent (0.5 μl of LgBiT protein + 0.1 μl of HiBiT Extracellular substrate + 50 μl of HiBiT Extracellular buffer), and added to a 96-well plate. HiBiT signal was detected as described above.

Statistical analysis

Statistical analysis was performed using GraphPad Prism 9.4.1 and 10. For comparing the split-GFP signals, we used the unpaired t-test. For the statistical comparison of the relative ratio of MSP domain secretion level, we used the ordinary one-way ANOVA with Dunnett's multiple comparison test or the unpaired t-test. Both tests were also used to compare the percentage of extracellular $FLAG/HA^+$ cells. The number of experiments and *P* values are indicated in the Fig. legends. All the experiments were not randomized, and the investigators were not blinded to allocation during experiments and outcome assessment. No statistical methods were performed to predetermine sample size.

Immunoelectron microscopy analysis

For immunoelectron microscopy, S2 cells stably expressing FLAG-$Vap33^{WT}$-HA driven by the *Actin5C* promoter were established by transfecting S2 cells with the *pAc5-STABLE-FLAG-$Vap33^{WT}$-HA-T2A-Neo^R* plasmid, with 2000 μg/ml G-418 (Roche, 04727878001) being used for selection. The stable cells were fixed with the fixative, then embedded in agarose and prepared as previously described[54,55]. Briefly, the cell suspension contained in a 15 ml centrifuge tube was centrifuged to gather cell pellets. After removal of supernatant, cells were rinsed with 0.1 M phosphate buffer (PB) (pH 7.4) and spun down. The S2 cell pellet was suspended in 1 ml of 0.1 M PB and mixed with 3 ml of 5% low-melting point agarose solution contained in a 35-mm diameter Petri dish. The cell-agarose suspension was then mixed by stirring in the dish and cooled in a refrigerator to solidify the agarose. The hardened agarose was detached from the dish and cut into small blocks. For cryoprotection, agarose blocks were soaked consecutively in 0.4 M, 0.9 M, 1.5 M and 2.3 M sucrose solution, and finally in a mixture of 20% polyvinyl pyrrolidone (PVP) and 1.84 M sucrose solution (3 h each, 4 °C). Specimens were subsequently placed on sample pins, quickly frozen in liquid nitrogen and loaded into a cryochamber (EM FC7; Leica Microsystems, Nussloch, Germany) attached to an ultramicrotome (Ultracut EM UC7; Leica Microsystems). Semithin cryosections (thickness of 1 μm) were cut from frozen specimens in a low-temperature sectioning system using a diamond knife (Diatome, Biel, Switzerland), picked up using 2.3 M sucrose droplets on wire loops and mounted onto glass microscope slides. The sections were rinsed with PBS, incubated with 5% normal goat serum (1 h, 20 °C) for blocking, and subsequently with a rabbit polyclonal anti-FLAG antibody (Sigma, F7425) for 12 h at 20 °C. The sections were then rinsed with PBS and

incubated with Nanogold-labeled goat polyclonal anti-rabbit IgG (Nanoprobes, NY, USA) or FluoroNanogold-labeled goat polyclonal anti-rabbit IgG (Nanoprobes) for 3 h at 20 °C. After sections were rinsed with PBS, they were further fixed with 2% glutaraldehyde for 12 h at 4 °C and rinsed with 0.1 M PB. To visualize the labeled-Nanogold by scanning electron microscopy, sections were incubated in the gold enhancing solution (GOLDENHANCE™ EM; Nanoprobes, NY, USA) for 3 min at 20 °C. Subsequently, they were further fixed with 2% osmium tetroxide for 1 h at 4 °C, stained with 1% aqueous uranyl acetate for 10 min, dehydrated in a graded ethanol series, and embedded in epoxy resin at 60 °C for 48 h. After semithin sections embedded in resin blocks were peeled off from the glass microscope slides, ultrathin sections were cut using a diamond knife (Diatome) and attached to glass slides by heating on a hot plate at 60 °C for 30 min. The ultrathin sections embedded in resin were heavy metal-stained with uranyl acetate and lead citrate, coated with carbon using a carbon coater (VC-100; Vacuum Device, Ibaraki, Japan) and finally observed using semi-in-lens type field emission scanning electron microscopes (SU-70 and Regulus: Hitachi, Tokyo, Japan).

Reporting summary

Further information on research design is available in the Nature Portfolio Reporting Summary linked to this article.

Data availability

The data supporting the findings of this study are available from the corresponding authors upon request. Source data are provided with this paper.

References

1. Kamemura, K. & Chihara, T. Multiple functions of the ER-resident VAP and its extracellular role in neural development and disease. *J. Biochem.* **165**, 391–400 (2019).
2. van Blitterswijk, M. et al. VAPB and C9orf72 mutations in 1 familial amyotrophic lateral sclerosis patient. *Neurobiol. Aging* **33**, 2950.e1–2950.e4 (2012).
3. Chen, H.-J. et al. Characterization of the properties of a novel mutation in VAPB in familial amyotrophic lateral sclerosis. *J. Biol. Chem.* **285**, 40266–40281 (2010).
4. Kabashi, E. et al. Investigating the contribution of VAPB/ALS8 loss of function in amyotrophic lateral sclerosis. *Hum. Mol. Genet.* **22**, 2350–2360 (2013).
5. Landers, J. E. et al. New VAPB deletion variant and exclusion of VAPB mutations in familial ALS. *Neurology* **70**, 1179–1185 (2008).
6. Nishimura, A. L. et al. A mutation in the vesicle-trafficking protein VAPB causes late-onset spinal muscular atrophy and amyotrophic lateral sclerosis. *Am. J. Hum. Genet.* **75**, 822–831 (2004).
7. Sun, Y. A novel mutation of VAPB in one Chinese familial amyotrophic lateral sclerosis pedigree and its clinical characteristics. *J. Neurol.* **264**, 2387–2393 (2017).
8. Soussan, L. et al. ERG30, a VAP-33-related protein, functions in protein transport mediated by COPI vesicles. *J. Cell Biol.* **146**, 301–311 (1999).
9. Diego, P., Nili, D., Eyal, S., Koret, H. & Sima, L. Coordinated lipid transfer between the endoplasmic reticulum and the Golgi complex requires the VAP proteins and is essential for Golgi-mediated transport. *Mol. Biol. Cell* **19**, 3871–3884 (2008).
10. Mikitova, V. & Levine, T. P. Analysis of the key elements of FFAT-like motifs identifies new proteins that potentially bind VAP on the ER, including two AKAPs and FAPP2. *PLoS One* **7**, e30455 (2012).
11. Mao, D. et al. VAMP associated proteins are required for autophagic and lysosomal degradation by promoting a PtdIns4P-mediated endosomal pathway. *Autophagy* **15**, 1214–1233 (2019).
12. Tsuda, H. et al. The amyotrophic lateral sclerosis 8 protein VAPB is cleaved, secreted, and acts as a ligand for Eph receptors. *Cell* **133**, 963–977 (2008).
13. Han, S. M. et al. Secreted VAPB/ALS8 major sperm protein domains modulate mitochondrial localization and morphology via growth cone guidance receptors. *Dev. Cell* **22**, 348–362 (2012).
14. Gkogkas, C. et al. VAPB interacts with and modulates the activity of ATF6. *Hum. Mol. Genet.* **17**, 1517–1526 (2008).
15. Gkogkas, C., Wardrope, C., Hannah, M. & Skehel, P. The ALS8-associated mutant VAPB P56S is resistant to proteolysis in neurons. *J. Neurochem.* **117**, 286–294 (2011).
16. Zein-Sabatto, H. et al. The type II integral ER membrane protein VAP-B homolog in C. elegans is cleaved to release the N-terminal MSP domain to signal non-cell-autonomously. *Dev. Biol.* **470**, 10–20 (2021).
17. Teuling, E. et al. Motor neuron disease-associated mutant vesicle-associated membrane protein-associated protein (VAP) B recruits wild-type VAPs into endoplasmic reticulum-derived tubular aggregates. *J. Neurosci.* **27**, 9801–9815 (2007).
18. Deidda, I. et al. Expression of vesicle-associated membrane-protein-associated protein B cleavage products in peripheral blood leukocytes and cerebrospinal fluid of patients with sporadic amyotrophic lateral sclerosis. *Eur. J. Neurol.* **21**, 478–485 (2014).
19. Ackerman, S. L. & Cox, G. A. From ER to Eph receptors: new roles for VAP fragments. *Cell* **133**, 949–951 (2008).
20. Zein-Sabatto, H., Collawn, J., Chang, C. & Miller, M. A. An RNAi screen in C. elegans for genes that play a role in secretion and cleavage of VAPB MSP domain. *bioRxiv* https://doi.org/10.1101/2021.01.02.425092 (2021).
21. McNew, J. A. et al. Ykt6p, a prenylated SNARE essential for endoplasmic reticulum-golgi transport. *J. Biol. Chem.* **272**, 17776–17783 (1997).
22. Zhang, T. & Hong, W. Ykt6 forms a SNARE complex with syntaxin 5, GS28, and Bet1 and participates in a late stage in endoplasmic reticulum-golgi transport. *J. Biol. Chem.* **276**, 27480–27487 (2001).
23. Gross, J. C., Chaudhary, V., Bartscherer, K. & Boutros, M. Active Wnt proteins are secreted on exosomes. *Nat. Cell Biol.* **14**, 1036–1045 (2012).
24. Nickel, W. & Rabouille, C. Mechanisms of regulated unconventional protein secretion. *Nat. Rev. Mol. Cell Biol.* **10**, 148–155 (2008).
25. Sebag, J. A. & Hinkle, P. M. Regions of melanocortin 2 (MC2) receptor accessory protein necessary for dual topology and MC2 receptor trafficking and signaling. *J. Biol. Chem.* **284**, 610–618 (2009).
26. Woodall, N. B., Yin, Y. & Bowie, J. U. Dual-topology insertion of a dual-topology membrane protein. *Nat. Commun.* **6**, 8099 (2015).
27. Cabantous, S., Terwilliger, T. C. & Waldo, G. S. Protein tagging and detection with engineered self-assembling fragments of green fluorescent protein. *Nat. Biotechnol.* **23**, 102–107 (2005).
28. Kamiyama, D. et al. Versatile protein tagging in cells with split fluorescent protein. *Nat. Commun.* **7**, 11046 (2016).
29. Kamiyama, R. et al. Cell-type-specific, multicolor labeling of endogenous proteins with split fluorescent protein tags in *Drosophila*. *Proc. Natl. Acad. Sci. USA.* **118**, e2024690118 (2021).
30. Lodish, H. et al. *Molecular Cell Biology* 6th edn (W.H. Freeman and Company) (2007).
31. Bogdanov, M. & Dowhan, W. Lipid-dependent generation of dual topology for a membrane protein. *J. Biol. Chem.* **287**, 37939–37948 (2012).
32. Chen, Q. et al. Inverting the topology of a transmembrane protein by regulating the translocation of the first transmembrane helix. *Mol. Cell* **63**, 567–578 (2016).
33. Hirai, Y. et al. Non-classical export of epimorphin and its adhesion to alphav-integrin in regulation of epithelial morphogenesis. *J. Cell Sci.* **120**, 2032–2043 (2007).
34. Gaspar, C. J. et al. EMC is required for biogenesis of Xport-A, an essential chaperone of Rhodopsin-1 and the TRP channel. *EMBO Rep.* **23**, e53210 (2022).

35. Bogdanov, M., Xie, J., Heacock, P. & Dowhan, W. To flip or not to flip: lipid-protein charge interactions are a determinant of final membrane protein topology. *J. Cell Biol.* **182**, 925–935 (2008).
36. Dowhan, W. & Bogdanov, M. Lipid-dependent membrane protein topogenesis. *Annu. Rev. Biochem.* **78**, 515–540 (2009).
37. Bard, F. et al. Functional genomics reveals genes involved in protein secretion and Golgi organization. *Nature* **439**, 604–607 (2006).
38. Kondylis, V. & Rabouille, C. A novel role for dp115 in the organization of tER sites in *Drosophila*. *J. Cell Biol.* **162**, 185–198 (2003).
39. Meyer, H. et al. *Drosophila* metalloproteases in development and differentiation: The role of ADAM proteins and their relatives. *Eur. J. Cell Biol.* **90**, 770–778 (2011).
40. Petri, J., Syed, M. H., Rey, S. & Klämbt, C. Non-cell-autonomous function of the GPI-anchored protein undicht during septate junction assembly. *Cell Rep.* **26**, 1641–1653.e4 (2019).
41. Saito, A. et al. Chondrocyte proliferation regulated by secreted luminal domain of ER stress transducer BBF2H7 / CREB3L2. *Mol. Cell* **53**, 127–139 (2014).
42. Rabouille, C. Pathways of unconventional protein secretion. *Trends Cell Biol.* **27**, 230–240 (2017).
43. Kang, F. et al. Plasma membrane flipping of Syntaxin-2 regulates its inhibitory action on insulin granule exocytosis. *Nat. Commun.* **13**, 6512 (2022).
44. Nilsson, I. & von Heijne, G. Fine-tuning the topology of a polytopic membrane protein: Role of positively and negatively charged amino acids. *Cell* **62**, 1135–1141 (1990).
45. Rutz, C., Rosenthal, W. & Schülein, R. A single negatively charged residue affects the orientation of a membrane protein in the inner membrane of Escherichia coli only when it is located adjacent to a transmembrane domain. *J. Biol. Chem.* **274**, 33757–33763 (1999).
46. Koch, C., Schuldiner, M. & Herrmann, J. M. ER-SURF: riding the endoplasmic reticulum surface to mitochondria. *Int. J. Mol. Sci.* **22**, 9655 (2021).
47. Huang, Z., Feng, Z. & Zou, Y. New wine in old bottles: current progress on P5 ATPases. *FEBS J.* **289**, 7304–7313 (2022).
48. Maricchiolo, E. et al. Unconventional pathways of protein secretion: mammals vs. plants. *Front. Cell Dev. Biol.* **10**, 895853 (2022).
49. Sánchez-Torres, J. L. et al. Matrix metalloproteinases deregulation in amyotrophic lateral sclerosis. *J. Neurol. Sci.* **419**, 117175 (2020).
50. Sokolowska, B., Jozwik, A., Niebroj-Dobosz, I., Janik, P. & Kwiecinski, H. Evaluation of matrix metalloproteinases in serum of patients with amyotrophic lateral sclerosis with pattern recognition methods. *J. Physiol. Pharmacol.* **60**, 117–120 (2009).
51. Rodríguez, D., Morrison, C. J. & Overall, C. M. Matrix metalloproteinases: What do they not do? New substrates and biological roles identified by murine models and proteomics. *Biochim. Biophys. Acta - Mol. Cell Res.* **1803**, 39–54 (2010).
52. Rogers, S. L., Rogers, G. C., Sharp, D. J. & Vale, R. D. *Drosophila* EB1 is important for proper assembly, dynamics, and positioning of the mitotic spindle. *J. Cell Biol.* **158**, 873–884 (2002).
53. Hu, Y. et al. UP-TORR: online tool for accurate and up-to-date annotation of RNAi reagents. *Genetics* **195**, 37–45 (2013).
54. Koga, D., Nakajima, M. & Ushiki, T. A useful method for observing intracellular structures of free and cultured cells by scanning electron microscopy. *J. Electron Microsc. (Tokyo)* **61**, 105–111 (2012).
55. Kusumi, S., Koga, D., Watanabe, T. & Shibata, M. Combination of a cryosectioning method and section scanning electron microscopy for immuno-scanning electron microscopy. *Biomed. Res.* **39**, 21–25 (2018).

Acknowledgements

We thank Hiroshi Tsuda (Takeda Pharmaceutical Company), Hugo Bellen (Baylor College of Medicine), Masayuki Miura (The Univ of Tokyo), Liqun Luo (Stanford Univ), Bloomington Stock Center and Vienna *Drosophila* Resource Center for fly stocks. We thank the *Drosophila* Genomics Resource Center (NIH Grant 2P40OD010949) for *CG30269, CG12012, CG17580, Syx13, and Sec61β* cDNA. We thank Satoko Okazaki and Miwako Kitamura for conducting immunostaining experiment for flow cytometry and lab members for active discussion. We thank Akiko Satoh for giving us S2 cells. We thank Editage (www.editage.jp) for English language editing. This work was supported by the Frontier Development Program for Genome Editing, Astellas Foundation for Research on Metabolic Disorders, Naito Foundation, JSPS KAKENHI (grant numbers 21H02479 and 21K18236) to T.C., JSPS KAKENHI (grant number 20K15903) and AMED (grant number JP22gm6310003) to M.O., The Akiyama Life Science Foundation to D.Koga, and NIH R01 NS107558 to D.Kamiyama, and JSPS Research Fellows (grant number 21J12274) and Yoshida Scholarship Foundation to K.K.

Author contributions

K.K. and T.C. conceived this project. K.K. and R.K. performed the experiments except immunoelectron microscopy analysis and HiBiT assay experiments. D.Kamiyama and S.S. contributed to Split-GFP experiments. D.Koga and S.K. carried out immunoelectron microscopy analysis. K.T., A.O., and M.T. performed HiBiT assay, immunostaining, and western blotting experiments, respectively. T.C. and M.O. supervised this project. The manuscript was written by K.K. and T.C. with input from all authors.

Competing interests

The authors declare no competing interests.

Additional information

Supplementary information The online version contains supplementary material available at https://doi.org/10.1038/s41467-024-53097-5.

Correspondence and requests for materials should be addressed to Takahiro Chihara.

Peer review information *Nature Communications* thanks Mikhail Bogdanov, and the other, anonymous, reviewer(s) for their contribution to the peer review of this work. A peer review file is available.